Supporting Information Organic Letters

Polarized Naphthalimide CH Donors Enhance Cl^- Binding Within an Aryl-Triazole Receptor

Kevin P. McDonald, Raghunath O. Ramabhadran, Semin Lee, Krishnan Raghavachari, Amar H. Flood*
Department of Chemistry, Indiana University, 800 East Kirkwood Avenue, Bloomington, IN 47405, USA
Email of corresponding author: aflood@indiana.edu

S1. General Methods

All reagents were obtained from commercial suppliers and used as received unless otherwise noted. 3-Nitro-1,8-naphthalic anhydride (**6**),[S1] 1-heptylhexylamine[S2], and 4-*tert*-butyl-azidobenzene (**9**),[S3] were prepared according to their literature procedures. Column chromatography was performed on silica gel (160 – 200 mesh), and thin-layer chromatography (TLC) was performed on precoated silica gel plates (0.25 mm thick, 60F254, Merck, Germany) and observed under UV light. Nuclear magnetic resonance (NMR) spectra were recorded on Varian Inova (400 MHz), Varian VXR (400 MHz) and Varian Gemini (300 MHz) spectrometers at room temperature (298 K). Chemical shifts were referenced on tetramethylsilane (TMS) or residual solvent peaks. High resolution electrospray ionization (ESI) mass spectrometry was performed on a Thermo Electron Corporation MAT 95XP-Trap mass spectrometer.

S2. Syntheses and Compound Characterization

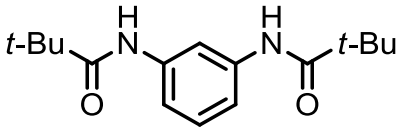

5

***N,N'*-(1,3-phenylene)bis(2,2-dimethylpropanamide) (5)**: *m*-Phenylenediamine (1.00 g, 9.25 mmol) was dissolved in dry THF (30 mL), triethylamine (7 mL) and was cooled to 0 °C. Trimethylacetyl chloride (2.45 g, 20.4 mmol) was dissolved in dry THF (15 mL) and added dropwise to the cooled *m*-phenylenediamine solution. After addition was complete, the solution was stirred at 0 °C for one hour and slowly warmed to room temperature. The resulting suspension was filtered over Celite and then washed with THF. The solution was concentrated, dissolved in dichloromethane, washed with $NaHCO_3$ (aq), brine, and then dried over $MgSO_4$. The resulting solution was concentrated and chromatographed over SiO_2 (10% acetone in dichloromethane) to yield **5** (2.44 g, 8.83mol, 95%) as a white solid. ^{1}H NMR (400 MHz, $CDCl_3$) δ = 7.90 (s, 1H), 7.42 (s, 2H), 7.29 (d, J = 7.0 Hz, 2H), 7.23 (t, J = 7.4 Hz, 1H), 1.30 (s, 18H). ^{13}C NMR (100 MHz, $CDCl_3$) δ = 176.78, 138.57, 129.33, 115.43, 111.33, 39.6, 27.5. HR-ESI-MS: $C_{16}H_{24}N_2O_2$ [M + Na^+], Calculated: 299.1735, Found: 299.1740.

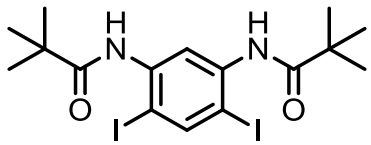

5'

***N,N'*-(4,6-diiodo-1,3-phenylene)bis(2,2-dimethylpropanamide) (5')**: **5** (2.44 g, 8.82 mmol) was dissolved in chloroform (75 mL) and warmed to 60 °C. Iodine monochloride (3.6 g, 22.0 mmol) was then added and the solution was stirred for 24 hours. After cooling to room temperature, the solution was then washed with Na_2CO_3 (aq), $Na_2S_2O_3$ (aq), and brine. After drying over $MgSO_4$, the solvent was removed and the crude material was chromatographed over SiO_2 (3% acetone in dichloromethane) to yield **5'** (5.89 g, 8.29 mol, 94%) as an off-white

solid. ^{1}H NMR (400 MHz, $CDCl_3$) δ = 9.07 (s, 1H), 8.04 (s, 1H), 7.74 (s, 2H), 1.35 (s, 18H). ^{13}C NMR (100 MHz, $CDCl_3$) δ = 176.32, 145.70, 139.23, 115.42, 84.42, 40.1, 27.6. HR-ESI-MS: $C_{16}H_{22}N_2O_2I_2$ [M + H^+], Calculated: 528.9849, Found: 528.9847.

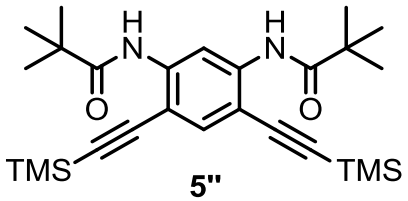

5"

***N,N*'-(4,6-bis((trimethylsilyl)ethynyl)-1,3-phenylene)bis(2,2-dimethylpropanamide) (5"): 5'** (1.00 g, 1.89 mmol) was dissolved in degassed, dry THF (50 mL). To the solution was added $PdCl_2(PPh_3)_2$ (66 mg, 0.095 mmol), CuI (18 mg, 0.095 mmol), trimethylsilylacetylene (555 mg, 5.67 mmol), and diisopropylamine (1.5 mL). The solution was stirred for 3 hours at room temperature and then filtered over Celite. After removal of the solvent, the resulting residue was chromatographed over SiO_2 (5% acetone in dichloromethane) to provide **5"** (880 mg, 1.87 mmol, 99% yield) as a yellow, waxy solid. ^{1}H NMR (300 MHz, $CDCl_3$) δ = 9.65 (s, 1H), 8.36 (s, 2H), 7.51 (s, 1H), 1.32 (s, 18H), 0.27 (s, 18H). ^{13}C NMR (100 MHz, $CDCl_3$) δ = 175.9, 140.9, 134.5, 108.8, 106.2, 101.3, 99.4, 40.2, 27.5. HR-ESI-MS: $C_{26}H_{40}N_2O_2Si_2$ [M + H^+], Calculated: 469.2707, Found: 469.2724.

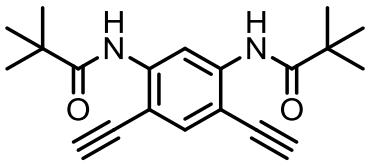

3

***N,N*'-(4,6-diethynyl-1,3-phenylene)bis(2,2-dimethylpropanamide) (3): 5"** (1.00 g, 2.11 mmol) was dissolved in THF (50 mL) and saturated K_2CO_3 in methanol (50 mL). The suspension was stirred for 15 minutes. H_2O was added (150 mL), followed by extraction with ethyl acetate and drying over $MgSO_4$. After removal of the solvent, the resulting residue was chromatographed over SiO_2 (10% ethyl acetate in hexanes) to provide **3** (580 mg, 1.78 mmol, 85% yield) as a brown solid. ^{1}H NMR (400 MHz, $CDCl_3$), δ = 9.64 (s, 1H), 8.31 (s, 2H), 7.53 (s, 1H), 3.50 (s, 2H), 1.32 (s, 18H). ^{13}C NMR (100 MHz, $CDCl_3$) δ = 176.2, 141.3, 135.0, 109.5, 105.3, 84.1, 78.4, 40.3, 27.5. HR-ESI-MS: $C_{20}H_{24}N_2O_2$ [M + H^+], Calculated: 325.1916, Found: 325.1900.

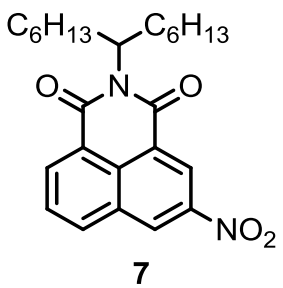

7

***N*-(1-hexylheptyl)-3-nitro-1,8-naphthalimide (7):** 3-Nitro-1,8-naphthalic anhydride[S1] (**6**) (1.08g, 4.44 mmol) was dissolved in pyridine (30 mL) and warmed to 100 °C. 1-heptylhexylamine (1.17 g, 5.77 mmol) in pyridine (10 mL) was then added dropwise. The resulting mixture was refluxed at 130 °C for 18 hours. The solution was then cooled and after removal of the solvent, the resulting residue was dissolved in dichloromethane, washed with 2 M HCl, brine, and then dried over $MgSO_4$. After removal of the solvent, the resulting residue was chromatographed over SiO_2 (10% ethyl acetate in hexanes) to afford **7** (1.11g, 2.61 mmol, 60%) as a brown oil. ^{1}H NMR (400 MHz, $CDCl_3$) δ = 9.24 (m, 1H), 9.12 (d, J = 2.4 Hz, 1H), 8.74 (m, 1H), 8.44 (d, J 8.2 Hz, 1H), 7.95 (t, J = 7.8 Hz, 1H), 5.14 (m, 1H), 2.18 (m, 2H), 1.82 (m, 2H), 1.31-1.12 (m, 16H), 0.77 (t, J = 7.0 Hz, 6H). ^{13}C NMR (125 MHz, $CDCl_3$) δ = 164.20, 163.59, 163.07, 162.40, 146.31, 135.13, 134.66, 133.95, 130.83, 130.24, 128.99, 128.48, 125.21, 124.45, 123.74, 123.06, 54.95, 32.15, 31.60, 29.06, 26.74, 22.45, 13.90 HR-ESI-MS: $C_{25}H_{35}N_2O_2$ [M+H$^+$] Calculated: 425.2440, Found: 425.2457.

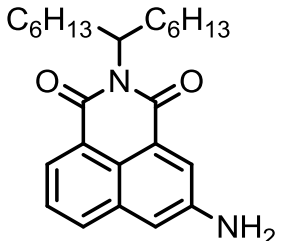

8

***N*-(1-hexylheptyl)-3-amino-1,8-naphthalimide (8):** **7** (620 mg, 1.46 mmol) were dissolved in a mixture of ethyl acetate (60 mL) and ethanol (20 mL), warmed to 60 °C and degassed with argon. $SnCl_2 \cdot 2H_2O$ (1.64 g, 7.3 mmol) was then added and the reaction mixture was stirred for 10 hours at 60 °C. After cooling, the solution was concentrated and saturated Na_2CO_3 (aq) (150 mL) was then added. The resulting suspension was then extracted with ethyl acetate, washed with brine, and dried over $MgSO_4$. The dried organic layer was then concentrated and chromatographed over SiO_2 (20% ethyl acetate in hexanes) to yield **8** (608 mg, 1.54 mmol, 98%) as a yellow-orange oil. ^{1}H NMR (400 MHz, $CDCl_3$) δ = 8.31 (m, 1H), 8.11 (m, 1H), 7.86 (d, J = 8.2 Hz, 1H), 7.56 (t, J = 7.5 Hz, 1H), 7.28 (d, J = 2.4 Hz, 1H), 5.18 (m, 1H), 4.42 (s, 2H), 2.22 (m, 2H), 1.82 (m, 2H), 1.33-1.21 (m, 16H), 0.81 (t, J = 7.1 Hz, 6H). ^{13}C NMR (125 MHz, $CDCl_3$) δ = 165.59, 165.42, 164.56, 164.30, 145.54, 133.21, 131.12, 127.50, 126.99, 126.72, 124.08, 123.35, 122.97, 122.49, 122.40, 122.22, 121.68, 113.37, 54.19, 32.33, 31.61, 29.10, 26.78, 22.43, 13.88. HR-ESI-MS: $C_{25}H_{35}N_2O_2$ [M + H$^+$], Calculated: 395.2699, Found: 395.2707.

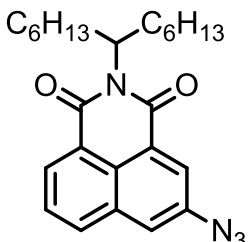

4

***N*-(1-hexylheptyl)-3-azido-1,8-naphthalimide (4):** **8** (450 mg, 1.14 mmol) was dissolved in acetonitrile (50 mL), water (30 mL), concentrated H_2SO_4 (10 mL) and cooled to 0 °C in an ice bath. $NaNO_2$ (236 mg, 3.42 mmol) in H_2O (5 mL) was then added dropwise. The solution was stirred for 15 minutes followed by the addition of NaN_3 (370 mg, 5.70 mmol) in H_2O (10 mL). The solution was warmed to 60 °C for 90 minutes and then cooled. Once cooled, the solution was extracted with ethyl acetate, washed with Na_2CO_3 (aq), $Na_2S_2O_3$ (aq), brine, dried over $MgSO_4$, and concentrated. The resulting residue was chromatographed over SiO_2 (15% ethyl acetate/hexanes) to provide **4** (466 mg, 1.11 mol, 97%) as a red-orange oil. ^{1}H NMR (500 MHz, $CDCl_3$) δ = 8.47 (m, 1H), 8.21 (m, 1H), 8.05 (d, J = 8.3 Hz, 1H), 7.71 (t, J = 8.2 Hz), 7.69(d, J = 2.4 Hz, 1H), 5.15 (m, 1H), 2.21 (m, 2H), 1.81 (m, 2H), 1.33-1.19 (m, 16H), 0.81 (t, J = 6.4 Hz, 6H). ^{13}C NMR (125 MHz, $CDCl_3$) δ = 164.82, 164.40, 163.74, 163.27, 139.36, 132.437, 132.20, 130.56, 129.81, 127.88, 125.66, 125.13, 124.45, 123.33, 122.54, 120.74, 54.55, 32.25, 31.64, 29.09, 26.78, 22.46, 13.90. HR-ESI-MS: $C_{25}H_{33}N_4O_2$ [M + H^+], Calculated: 421.2604, Found: 421.2625.

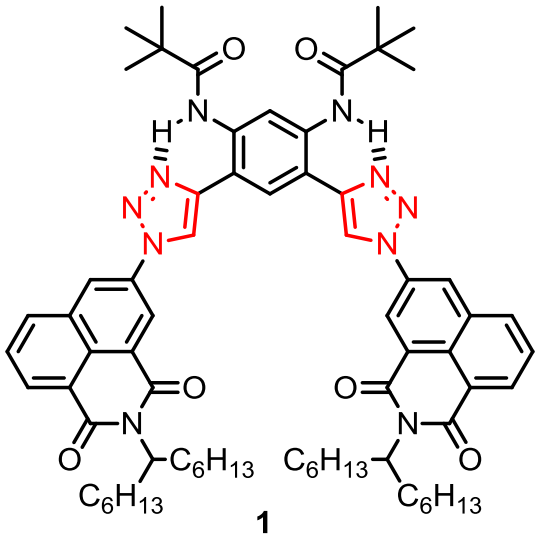

1

Receptor 1: **3** (51.1 mg, 0.160 mmol) and **4** (145 mg, 0.345 mmol) was dissolved in ethanol (10 mL), tetrahydrofuran (10 mL), and degassed with argon. After 15 minutes, $CuSO_4 \cdot 5H_2O$ (86.3 mg, 0.345 mmol) dissolved in H_2O (1 mL) and sodium ascorbate (68.7 mg, 0.346 mmol) dissolved in H_2O (1 mL) was added. The solution was stirred for 12 hours at 50 °C, cooled to 0 °C, and filtered. The precipitate was dissolved in dichloromethane, washed with brine, dried over $MgSO_4$ and chromatographed over SiO_2 (5% acetone in dichloromethane) to yield **1** (74 mg, 0.064 mmol, 40%) as a yellow, waxy solid. ^{1}H NMR (400 MHz, CD_2Cl_2) δ = 11.26 (s, 2H), 10.03 (s, 1H), 9.03 (s, 2H), 8.99 (s, 2H), 8.74 (s, 2H), 8.67 (s, 2H), 8.44 (d, J = 7.5 Hz, 2H), 7.90 (t, J = 7.4 Hz, 2H), 7.70 (s, 1H), 5.22 (m, 2H), 2.29 (m, 2H), 1.89 (m, 2H), 1.37 (s, 18H), 1.37-1.25 (m, 16H), 0.85 (m, 6H). ^{13}C NMR (125 MHz, CD_2Cl_2) δ = 178.19, 165.27, 164.95, 164.11, 163.77, 148.49, 138.30, 132.01, 131.44, 135.66, 134.55, 132.86, 132.66, 132.06, 129.11, 128.32, 126.20, 125.36, 124.39, 124.24, 123.47, 122.79, 119.42, 113.39, 112.73, 55.31, 40.95, 32.93, 32.36, 29.81, 28.05, 27.48, 23.16, 14.39. HR-ESI-MS: $C_{70}H_{88}N_{10}O_6$ [M + H^+], Calculated: 1165.6961, Found: 1165.6936.

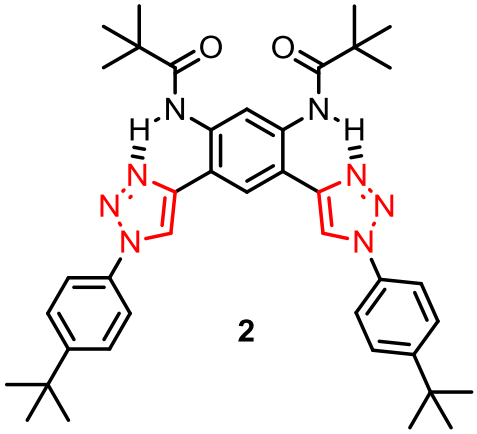

2

Receptor 2: **3** (50 mg, 0.15 mmol) and **9** (59 mg, 0.34 mmol) were dissolved in toluene (10 mL), degassed with argon and warmed to 60 °C. After degassing for 15 minutes, CuI (9.0 mg, 0.05 mmol) and 1,8-diazobicycloundec-7-ene (DBU, 150 μL) was added and the solution was stirred under argon for 12 hours at 60 °C. After cooling to room temperature, H_2O (100 mL) was added and the suspension was extracted with ethyl acetate. The resulting solution was washed with brine, dried over $MgSO_4$ and the solvent was removed. The crude residue was chromatographed over SiO_2 (5% acetone in hexanes) to yield **2** (42 mg, 0.062 mmol, 40%) as a white solid. ^{1}H NMR (500 MHz, $CDCl_3$) δ = 11.15 (s, 2H), 9.95 (s, 1H), 8.31 (s, 2H), 7.74 (d, J = 6.9 Hz, 2H), 7.66 (s, 1H), 7.56 (d, J = 6.8 Hz, 2H), 1.38 (s, 18H), 1.35 (s, 18 H). ^{13}C NMR (125 MHz, $CDCl_3$) δ = 177.54, 152.60, 147.51, 137.60, 134.29, 126.69, 125.75, 120.46, 118.57, 113.01, 109.99, 40.36, 34.85, 31.26, 27.72. HR-ESI-MS: $C_{40}H_{50}N_8O_2$ [M + H^+], Calculated: 675.4135, Found: 675.4103.

S3. ^{1}H and ^{13}C NMR Spectra (asterisks (*) indicate impurities)

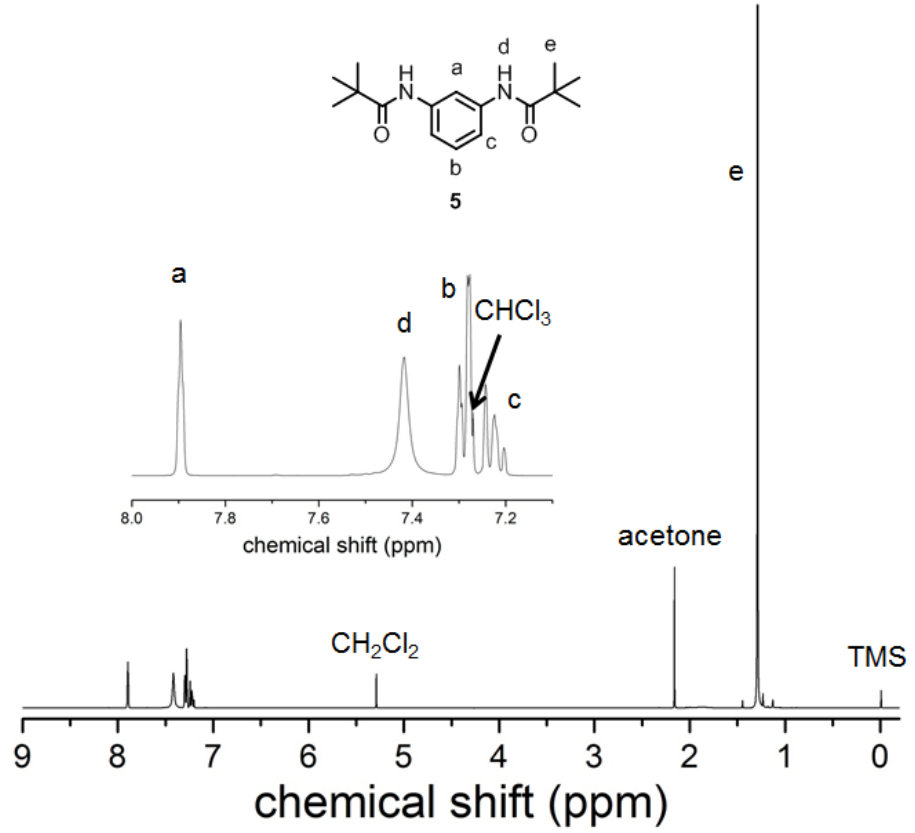

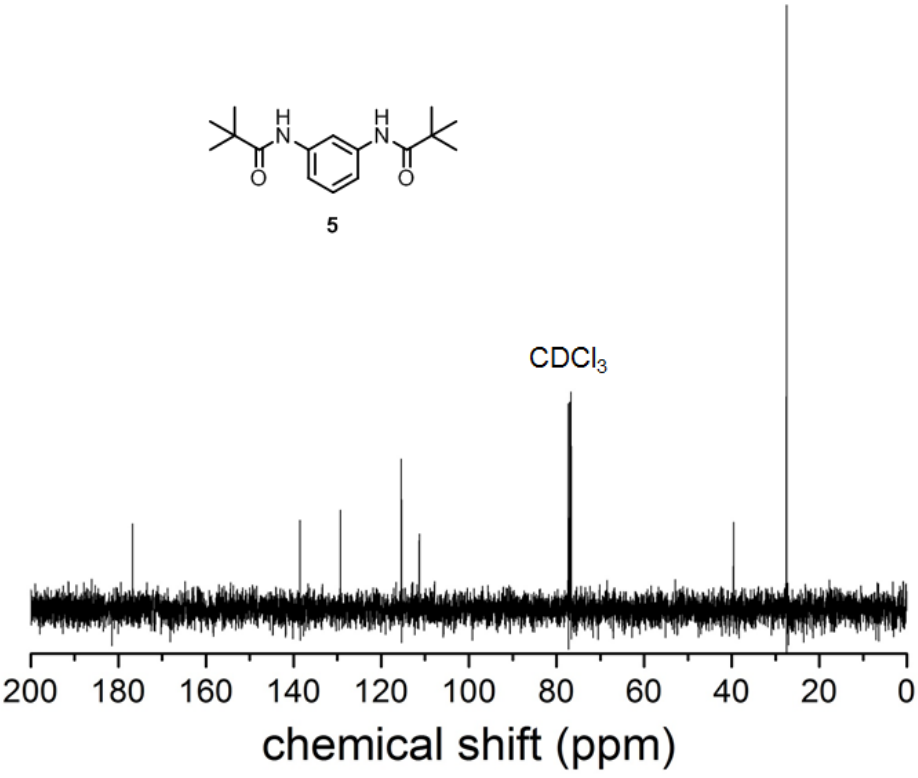

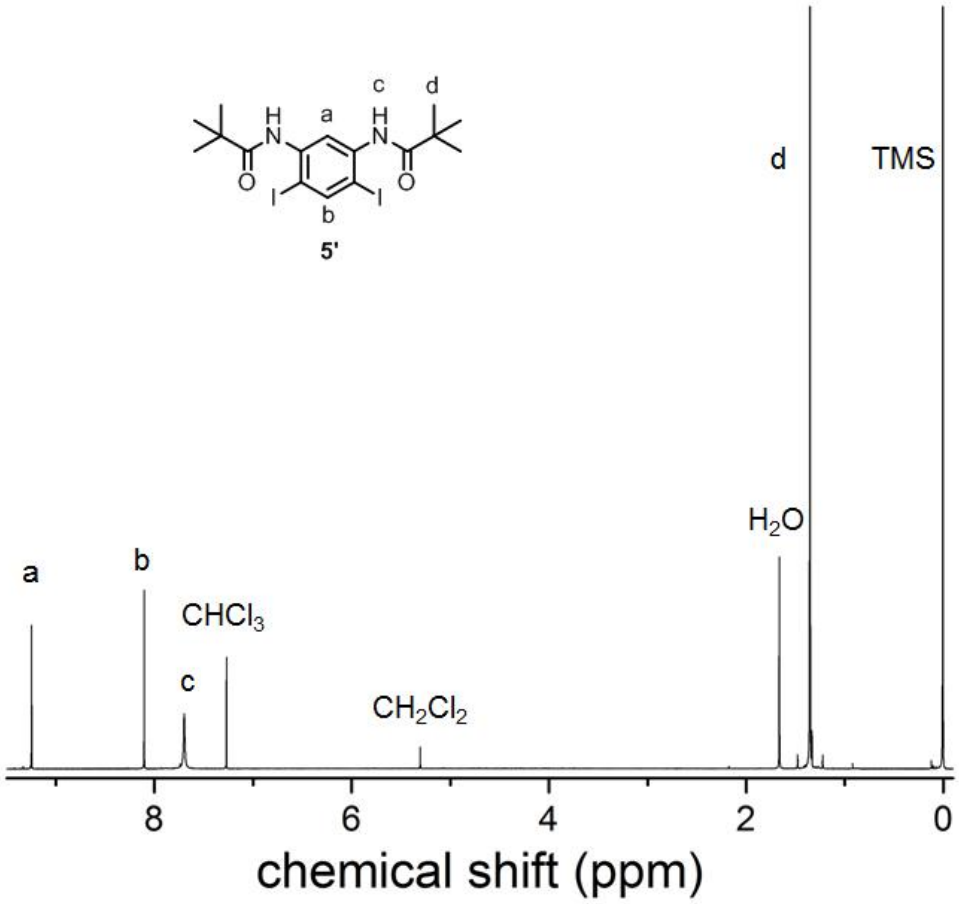
c
d
a
H
N
H
N
O
O
I
I
b
5'
d
TMS
H2O
a
b
CHCl3
c
CH2Cl2
8
6
4
2
0
chemical shift (ppm)

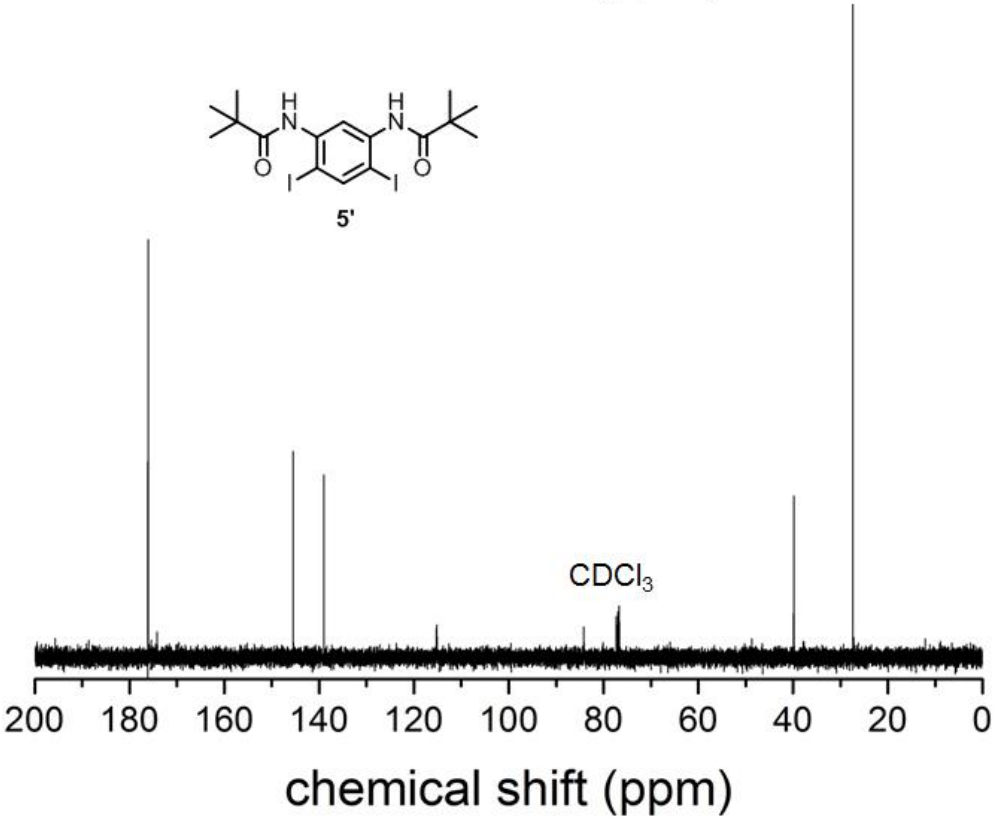
H
N
H
N
O
O
I
I
5'
CDCl3
200
180
160
140
120
100
80
60
40
20
0
chemical shift (ppm)

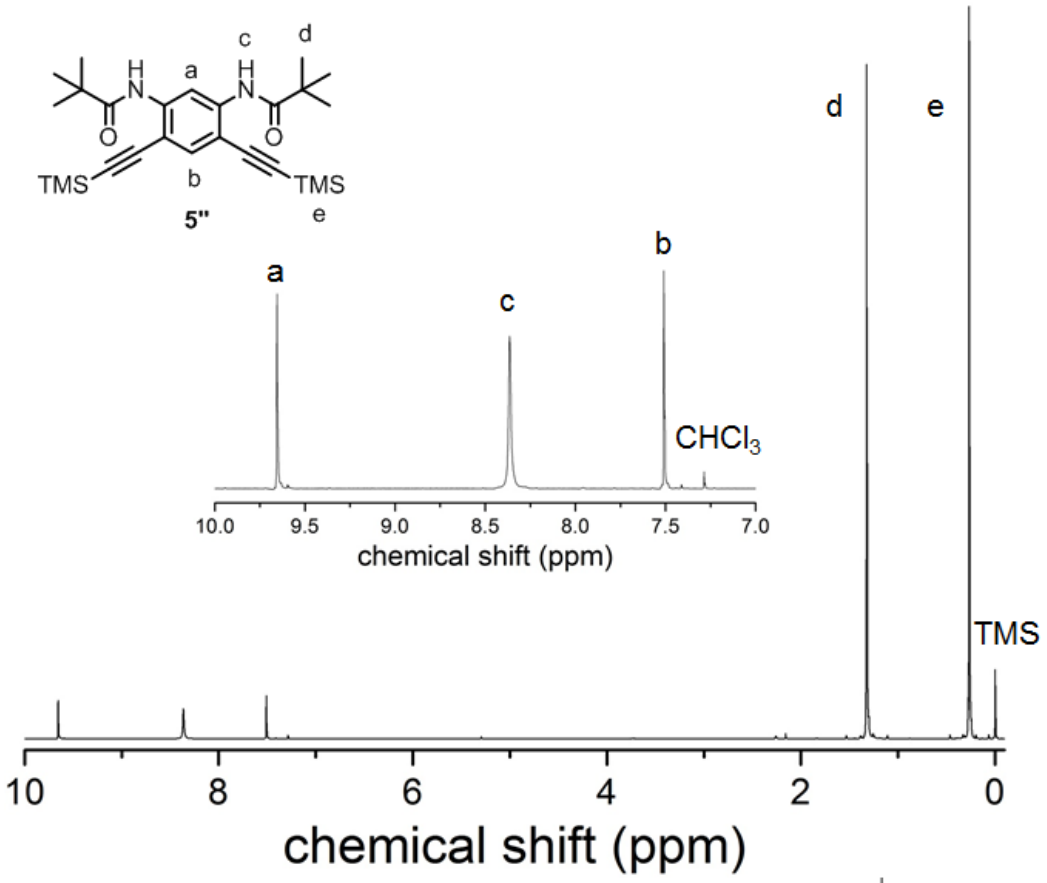
c
d
a
H
N
H
N
O
O
TMS
b
TMS
e
5"
d
e
a
c
b
CHCl3
10.0
9.5
9.0
8.5
8.0
7.5
7.0
chemical shift (ppm)
TMS
10
8
6
4
2
0
chemical shift (ppm)

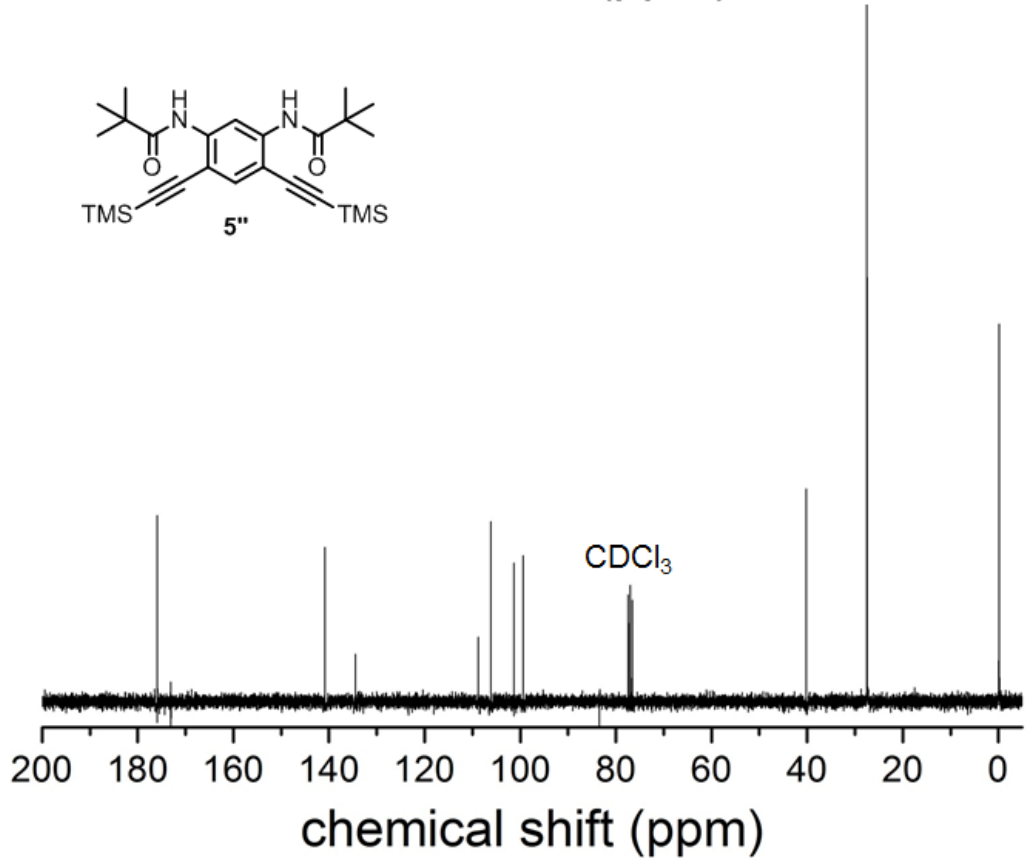
H
N
H
N
O
O
TMS
TMS
5"
CDCl3
200
180
160
140
120
100
80
60
40
20
0
chemical shift (ppm)

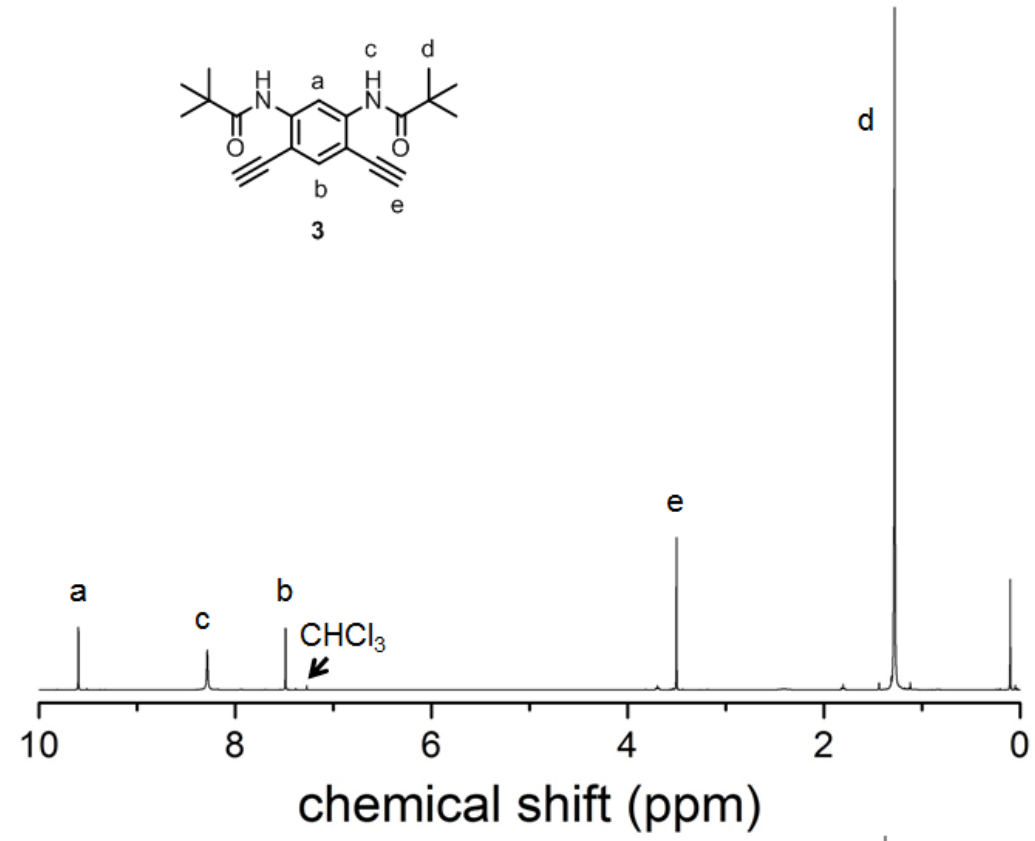
c
d
a
H
N
H
N
O
O
b
e
3
d
e
a
c
b
CHCl3
10
8
6
4
2
0
chemical shift (ppm)

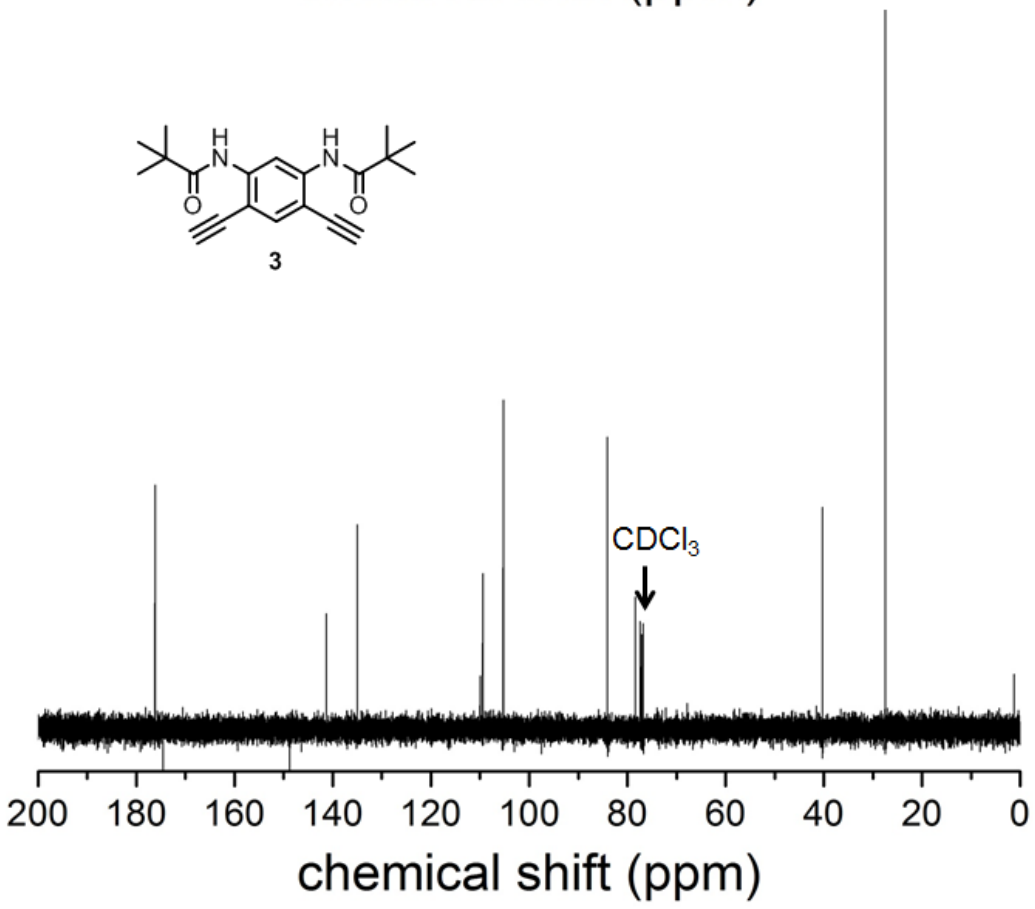
H
N
H
N
O
O
3
CDCl3
200
180
160
140
120
100
80
60
40
20
0
chemical shift (ppm)

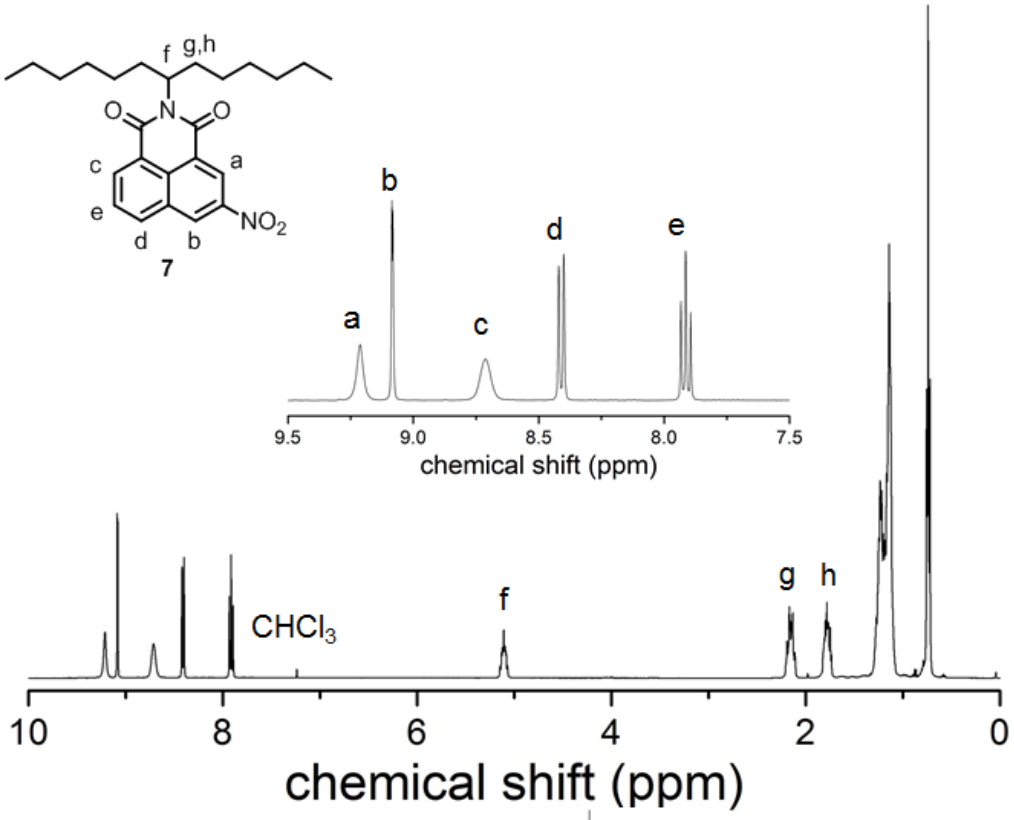
f
g,h
O
N
O
c
a
e
NO2
d
b
7
a
b
c
d
e
9.5
9.0
8.5
8.0
7.5
chemical shift (ppm)
CHCl3
f
g
h
10
8
6
4
2
0
chemical shift (ppm)

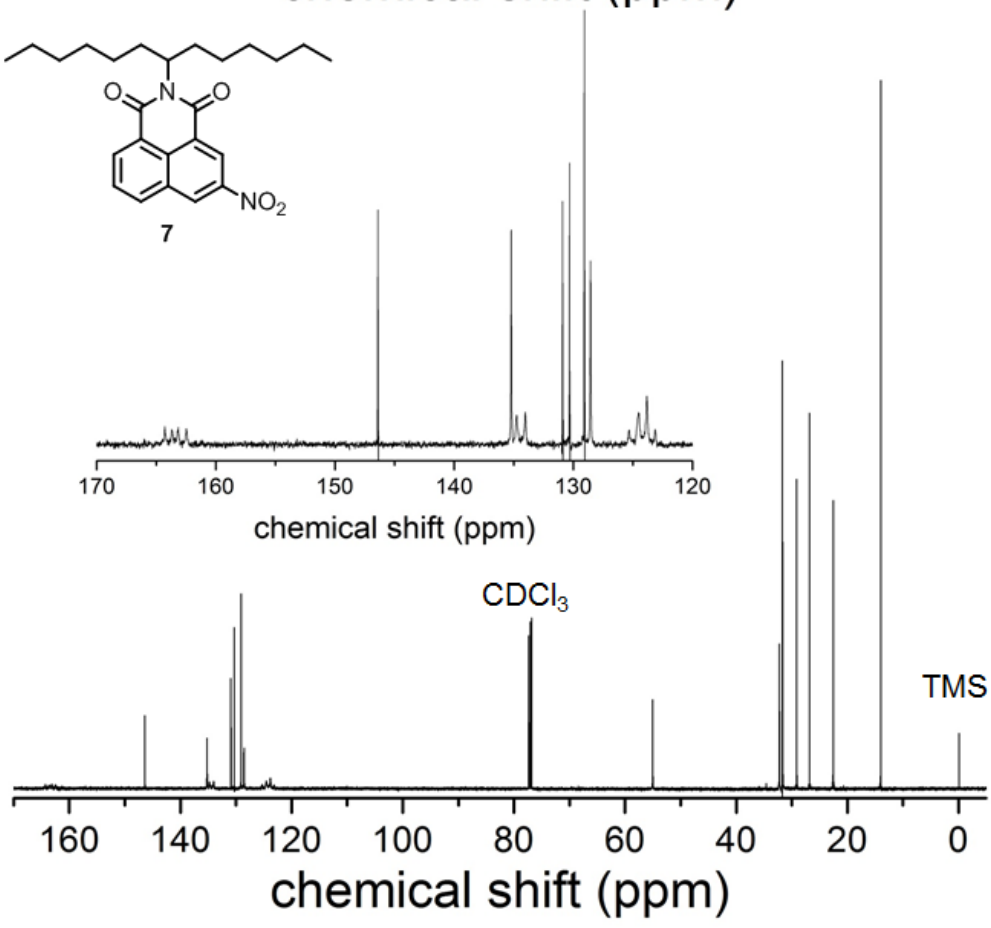
O
N
O
NO2
7
170
160
150
140
130
120
chemical shift (ppm)
CDCl3
TMS
160
140
120
100
80
60
40
20
0
chemical shift (ppm)

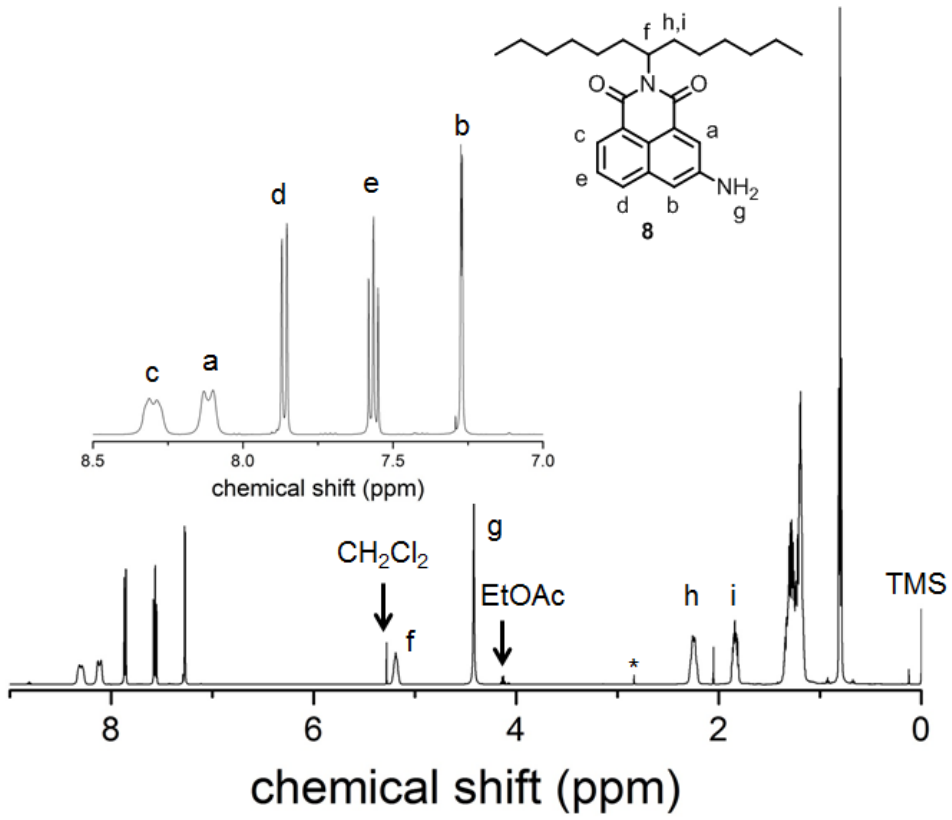
f
h,i
O
N
O
c
a
e
d
b
NH2
g
8
b
d
e
c
a
8.5
8.0
7.5
7.0
chemical shift (ppm)
g
CH2Cl2
EtOAc
h
i
TMS
f
*
8
6
4
2
0
chemical shift (ppm)

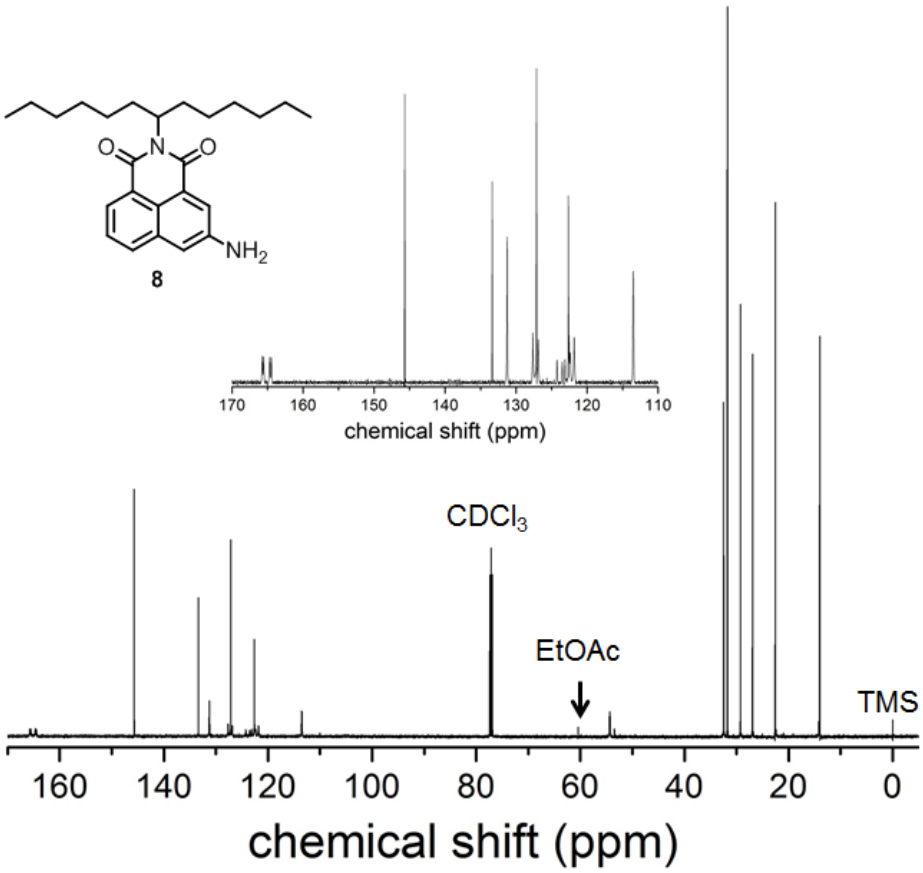
O
N
O
NH2
8
170
160
150
140
130
120
110
chemical shift (ppm)
CDCl3
EtOAc
TMS
160
140
120
100
80
60
40
20
0
chemical shift (ppm)

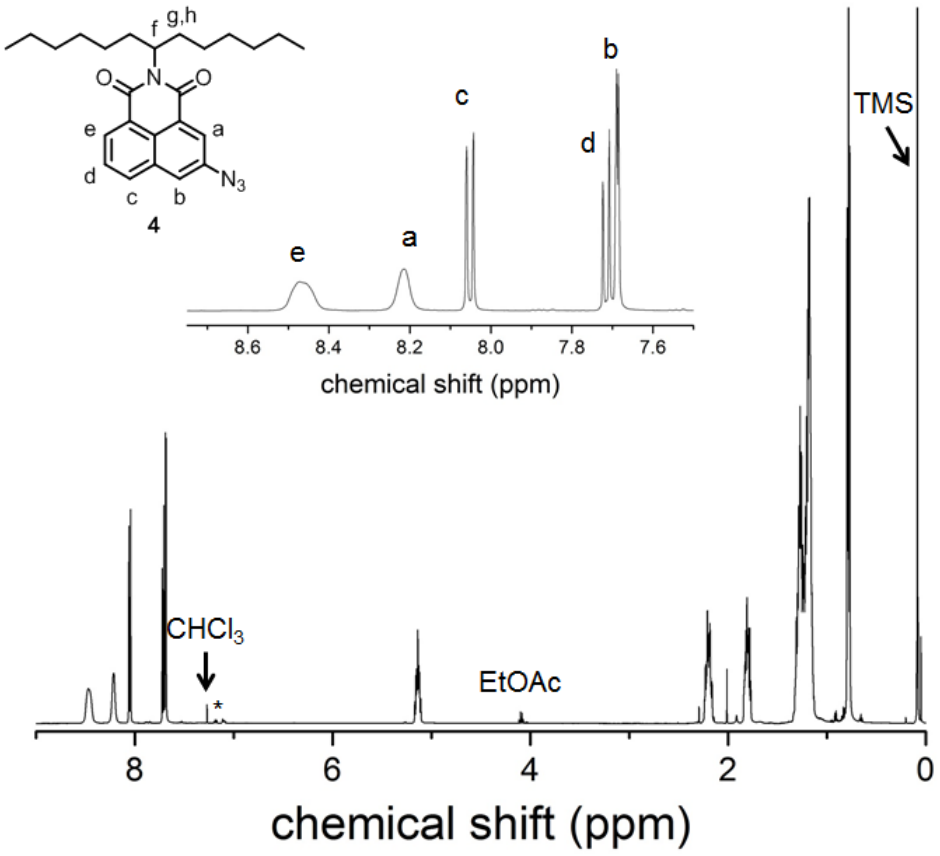
f
g,h
O
N
O
e
a
d
N_3
c
b
4
e
a
c
d
b
8.6
8.4
8.2
8.0
7.8
7.6
chemical shift (ppm)
TMS
$CHCl_3$
*
EtOAc
8
6
4
2
0
chemical shift (ppm)

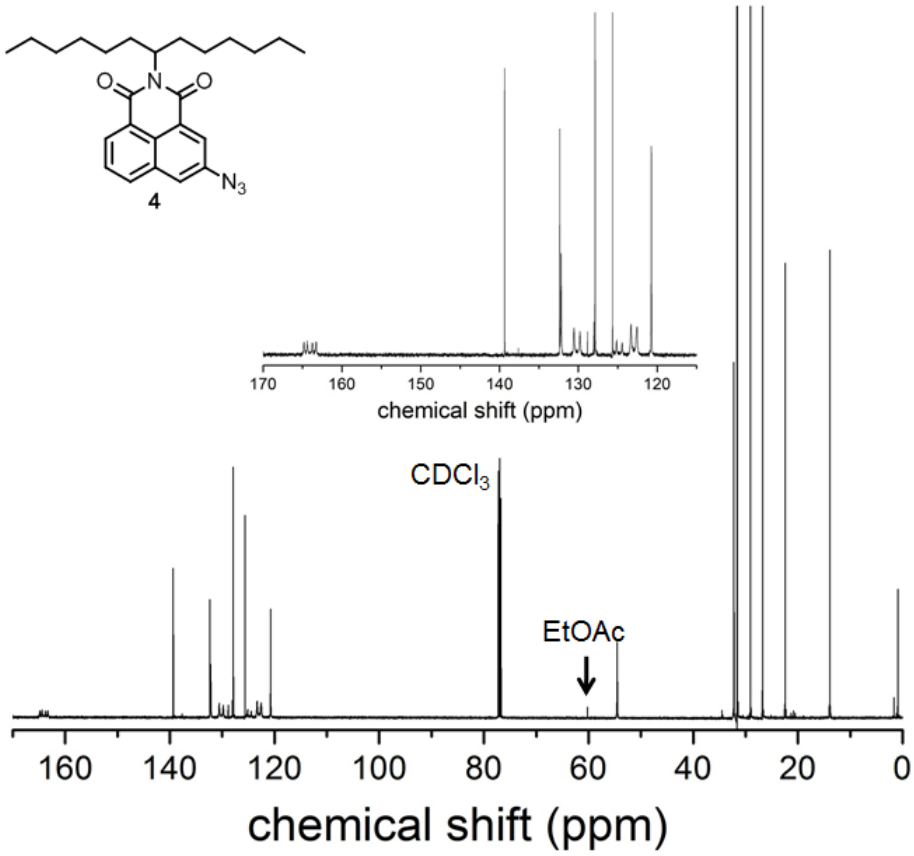
O
N
O
N_3
4
170
160
150
140
130
120
chemical shift (ppm)
$CDCl_3$
EtOAc
160
140
120
100
80
60
40
20
0
chemical shift (ppm)

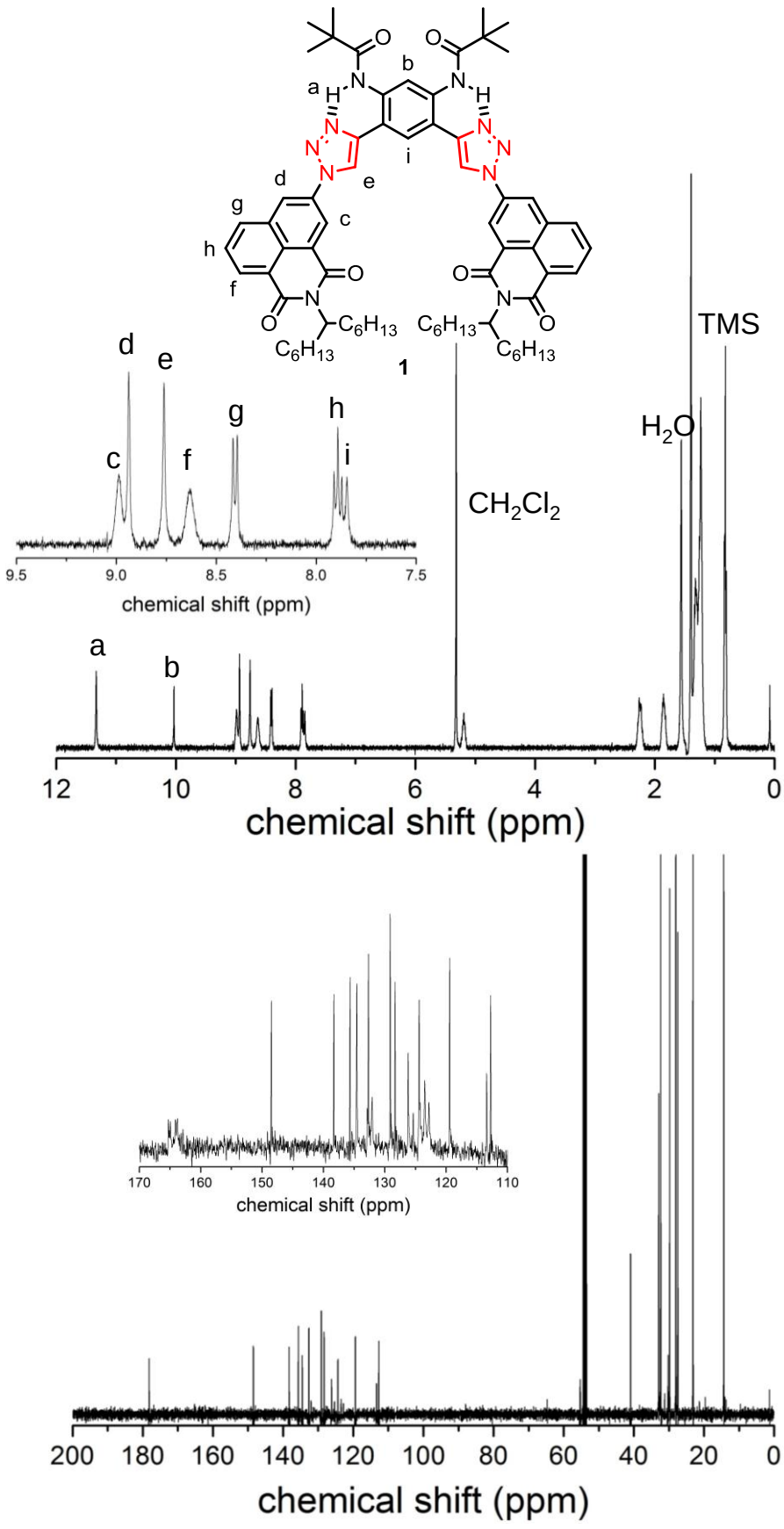
1
TMS
H_2O
CH_2Cl_2
chemical shift (ppm)
chemical shift (ppm)
chemical shift (ppm)

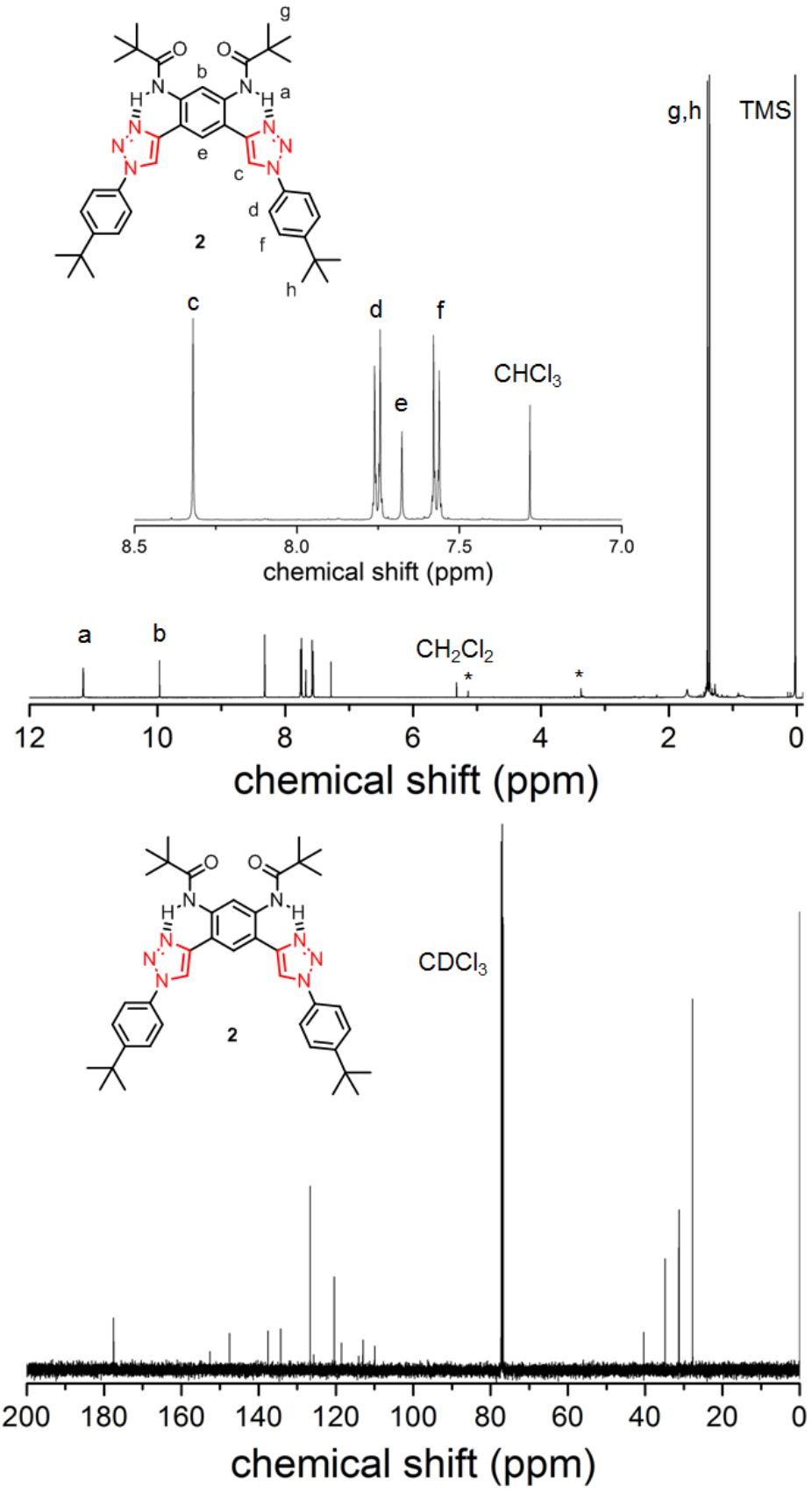
g
O
O
b
N
H
N
H
a
N
N
N
N
e
c
d
f
h
2
g,h
TMS
c
d
f
e
CHCl3
8.5
8.0
7.5
7.0
chemical shift (ppm)
a
b
CH2Cl2
*
*
12
10
8
6
4
2
0
chemical shift (ppm)
2
CDCl3
200
180
160
140
120
100
80
60
40
20
0
chemical shift (ppm)

S4. Conformational Analysis of 1 and 1•Cl⁻

As described in the main text, the lack of C_2 symmetry about the naphthalimide-triazole bond in **1** causes the free receptor to adopt conformations that are not suitable for anion binding. Herein, a conformational analysis combining both theoretical calculations and solution studies provides a qualitative understanding of the energetic penalties that receptor **1** must pay relative to control compound **2**.

In the absence of anion, free rotation about both naphthalimide-triazole bonds allows **1** to adopt four low-energy conformations (Figure S1). The "in" rotamer refers to when the polarized naphthalimide CH donors are directed towards the triazole CH (organized for anion binding) while the "out" rotamer orients those donors away from the electropositive cavity. The "out-out" conformer is expected to be the most stable while the "in-in" conformer is highest in energy as it converges the naphthalimide donors into the electropositive cavity outlined by the triazoles.

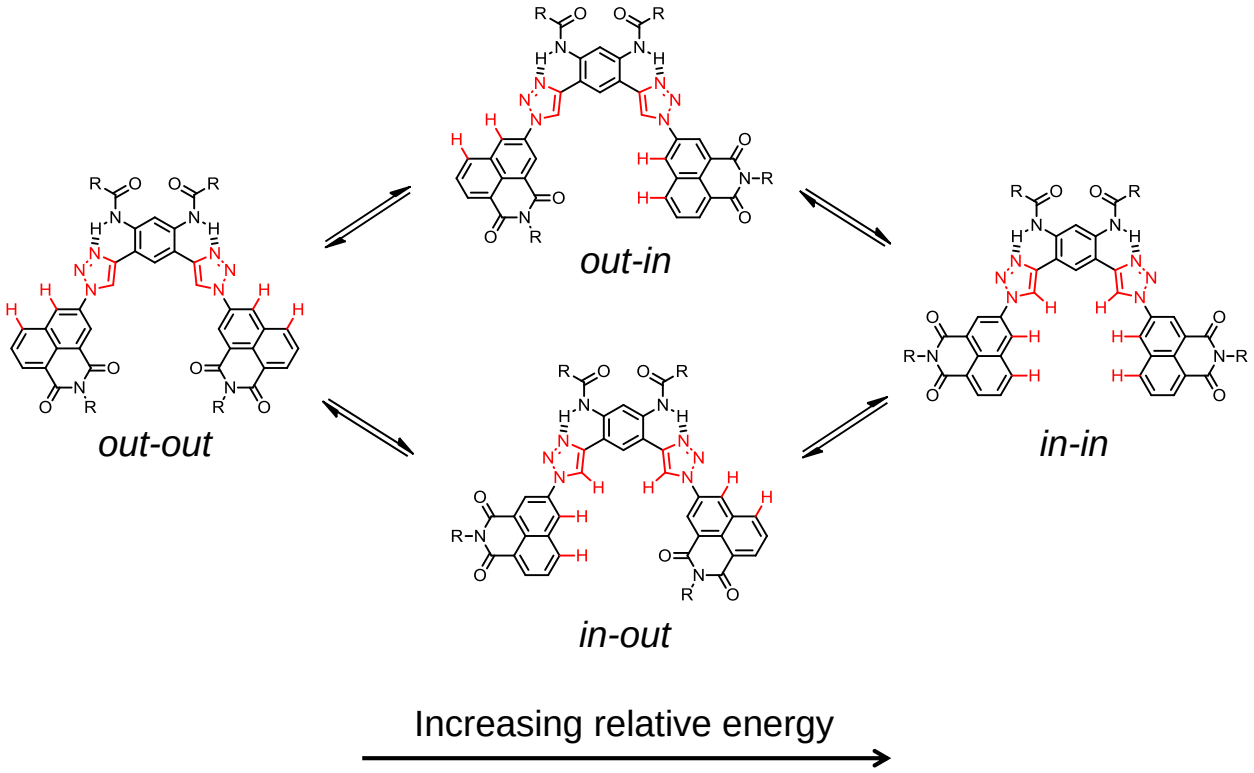

Figure S1. Receptor **1** can exist in one of four low-energy conformation in which the naphthalimide CH donors are syn (in) or anti (out) to the adjacent triazole CH donor. Calculations (HF/3-21G) showed that the "in-in" conformer is higher in energy presumably due to electrostatic repulsions between electropositive CH donors.

To explore these possible equilibria in solution, compound **S4** was prepared as a model system for the naphthalimide-triazole-phenyl triad of receptor **1**. Triad **S4** (Scheme S1) was prepared from azide **S3** and alkyne **S5**. Azide **S3** was prepared using similar conditions to those described in the main text.[S1] Alkyne **S5** was prepared according to known literature procedures.[S3] The 2D NOESY spectrum of **S4** (Figure S2) showed cross peaks for H_d-H_a and H_d-H_b consistent with both the "in" and "out" rotamers being present in at 298 K.

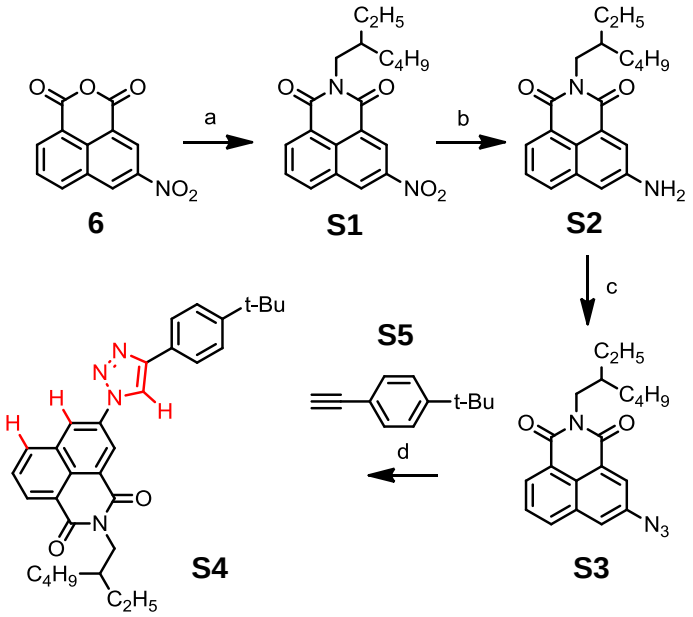

Scheme S1. Synthesis of compound **S4**: (a) 2-ethylhexylamine, EtOH, 80 °C; (b) $SnCl_2 \cdot 2H_2O$, EtOH, 60 °C; (c) *t*-BuONO, CH_3CN, then $TMSN_3$; (d) $CuSO_4 \cdot 5H_2O$, Na ascorbate, THF:EtOH:H_2O.

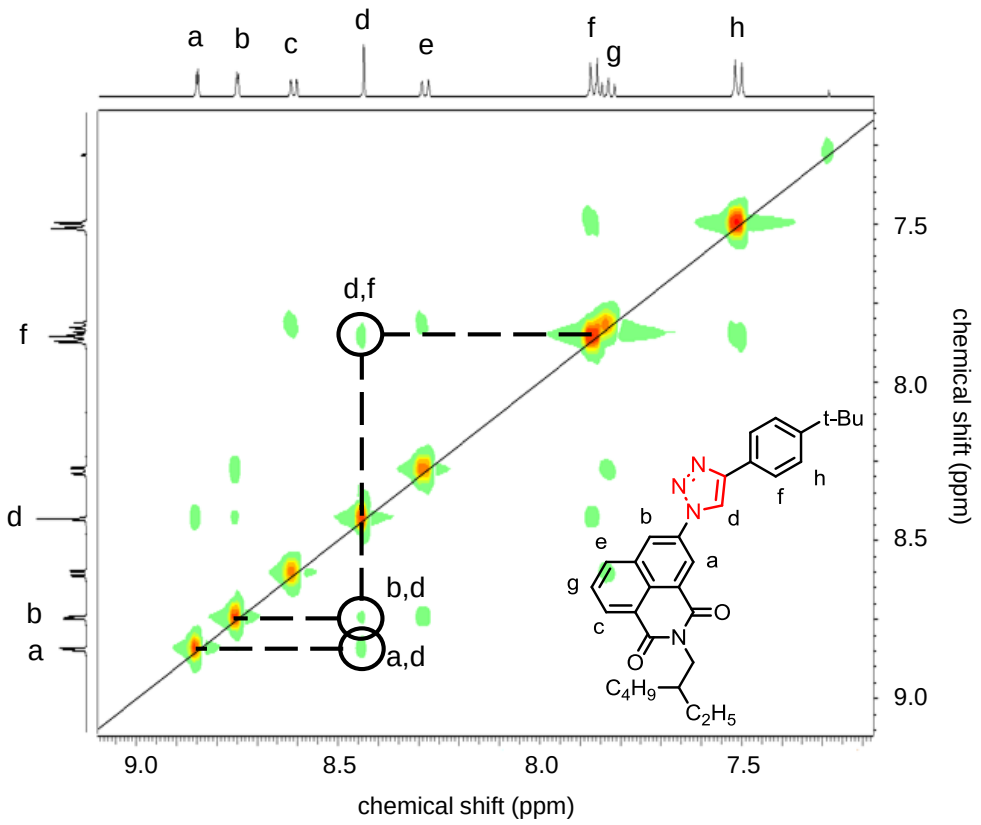

Figure S2. 2D NOESY spectrum of triad **S4** showing diagnostic correlation peaks that are consistent with free rotation about the naphthalimide-triazole bond.

While the NOESY experiment (Figure S2) hints at their relative population of these rotamers in solution, DFT calculations were performed to explore the energetic profile of their interconversion. The rotational barrier going from the "in" to the "out" rotamer of the naphthalimide sidearm was obtained by running a relaxed scan along the naphthalimide-triazole dihedral angle at the B3LYP/6-31+G(d,p) level of theory. A plot of the relative energies vs. the naphthalimide-triazole dihedral angle is shown over a full 360 degree rotation (Figure S3). A total of four minima (A-D) were observed. Conformations A and D correspond to the "in" rotamer while B and C are from the "out" rotamer. These double minima for each rotamer are a result of unwanted electrostatic repulsions between the hydrogens of the naphthalimide and triazole moieties. This finding is consistent with prior calculations on aryl-triazole scaffolds.[S4] Despite these double minima for each naphthalimide-triazole bond in **1**, the barrier between these are negligible (~1 kJ/mol), thus allowing the conformational space to be simplified to the four conformers depicted in Figure S1.

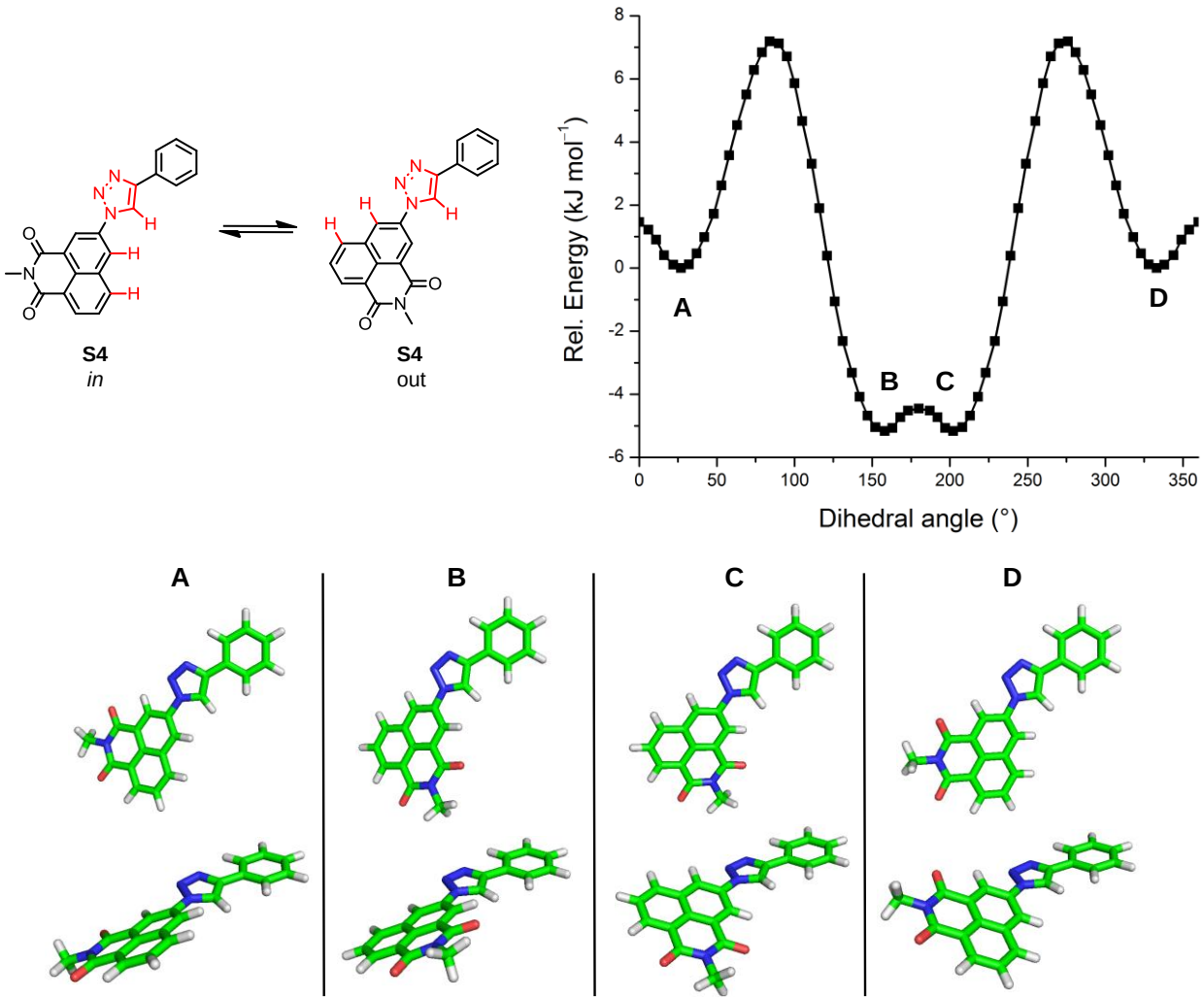

Figure S3. The relative energy (B3LYP/6-31+G(d,p)) of **S4** as a function of dihedral angle about the naphthalimide-triazole bond is shown across a full 360° rotation. The "out" rotamer (**B** and **C**) is favored by 5.2 kJ/mol relative to the "in" rotamer (**A** and **D**).

The lowest energy conformer for triad **S4** has a dihedral angle close to 180° (**B** 158°, **C** 202°) where the polarized naphthalimide CH donors are oriented away from the electropositive triazole CH avoiding unwanted dipole-dipole interactions and electrostatic repulsions. The "out" conformer is favored by 5.2 kJ/mol compared to the "in" conformer where these electropositive donors converge. The rotational barrier for converting the "out" to the "in" conformer was found to be 12.3 kJ/mol. Based on these gas-phase calculations and the experimental NOESY data on **S4**, it is rationalized that **1** adopts each conformation ("in" and "out") about the naphthalimide-triazole bond and the rotational barriers are such that these conformers are interconverting at room temperature. However, since the "in-in" conformer is the structure of the **1**•Cl^- complex, the expected electrostatic repulsions incur an enthalpic energetic penalty.

To provide evidence for the "in-in" conformer as the structure of the **1**•Cl^- complex, a 2D ROESY NMR investigation of **1** was obtained with added 10 equivalents TBACl (5 mM, CD_2Cl_2). Previous ^1H NMR titrations (not shown) at this higher concentration demonstrated receptor saturation of **1** with chloride in the presence of 10 equivalents TBACl. Diagnostic cross peaks consistent with the "in-in" conformer are observed between H_d and H_e. At the same time, this experiment provided assignments for all observed aromatic signals based on the H_d–H_i, H_d–H_g, and H_g–H_h cross peaks. Further support for the "in-in" conformation of **1**•Cl^- is also provided by the $\Delta\delta$ values for the naphthalimide resonances upon Cl^- binding. Proton H_d shifts to a greater extent (0.7 ppm) than H_c (~0.1 ppm) consistent with stronger hydrogen bonding interactions within the "in-in" conformer (Figure S13). Calculations (HF/3-21G) performed on **1**•Cl^- complex in both "in-in" and "out-in" conformers determined that the "in-in" conformer was favored by 35.2 kJ/mol.

Enthalpy and Entropy Adjustments

From the preceding conformational analysis and ignoring changes in solvation, receptor **1** must pay *two* added energetic penalties compared to **2** in order to bind anions. Enthalpically, the lowest energy rotamer ("out") about the naphthalimide-triazole bond orients the polarized CH donors away from the triazole donor. To overcome the electrostatic repulsions within the "in-in" conformer, an energetic penalty (5.2 kJ/mol) must be paid for *each* naphthalimide-triazole bond. By comparison, the C_2 symmetry about the terminal phenyl-triazole bond in **2** dictates that any low energy rotamer about this bond is its most suited for hydrogen bonding interactions with an added anion.

Entropically, both receptors have four low-energy conformations in the absence of anion deriving from two different rotamers about each aryl (naphthalimide or phenyl) triazole bond. Upon addition of a halide salt, the conformational space of naphthalimide receptor **1** is condensed to having only one observed conformation ("in-in") as supported by 2D ROESY NMR spectroscopy and $\Delta\delta$ values. This reduction in the number of conformations presents a conformational entropy penalty (ΔS_{conf}). As estimated in prior work,[S5] this may cost receptor **1** approximately 2-4 kJ/mol of binding affinity. For phenyl receptor **2**, its symmetry about the phenyl-triazole bond provides four degenerate conformations both before and after anion binding. If there was any perturbation in the rotation of the phenyl-triazole bond, it is expected that a splitting of the terminal phenylene resonances would be observed consistent with a loss of symmetry. Since there is no change in the symmetry of **2** upon anion binding (Figure S16-S18), this bond is freely rotating within the **2**•X^- complexes consistent with a minimal change in conformational entropy. While these enthalpy and entropy adjustments have been quantified in

the gas phase with DFT calculations, their values are taken as qualitative insights into what is taking place in solution.

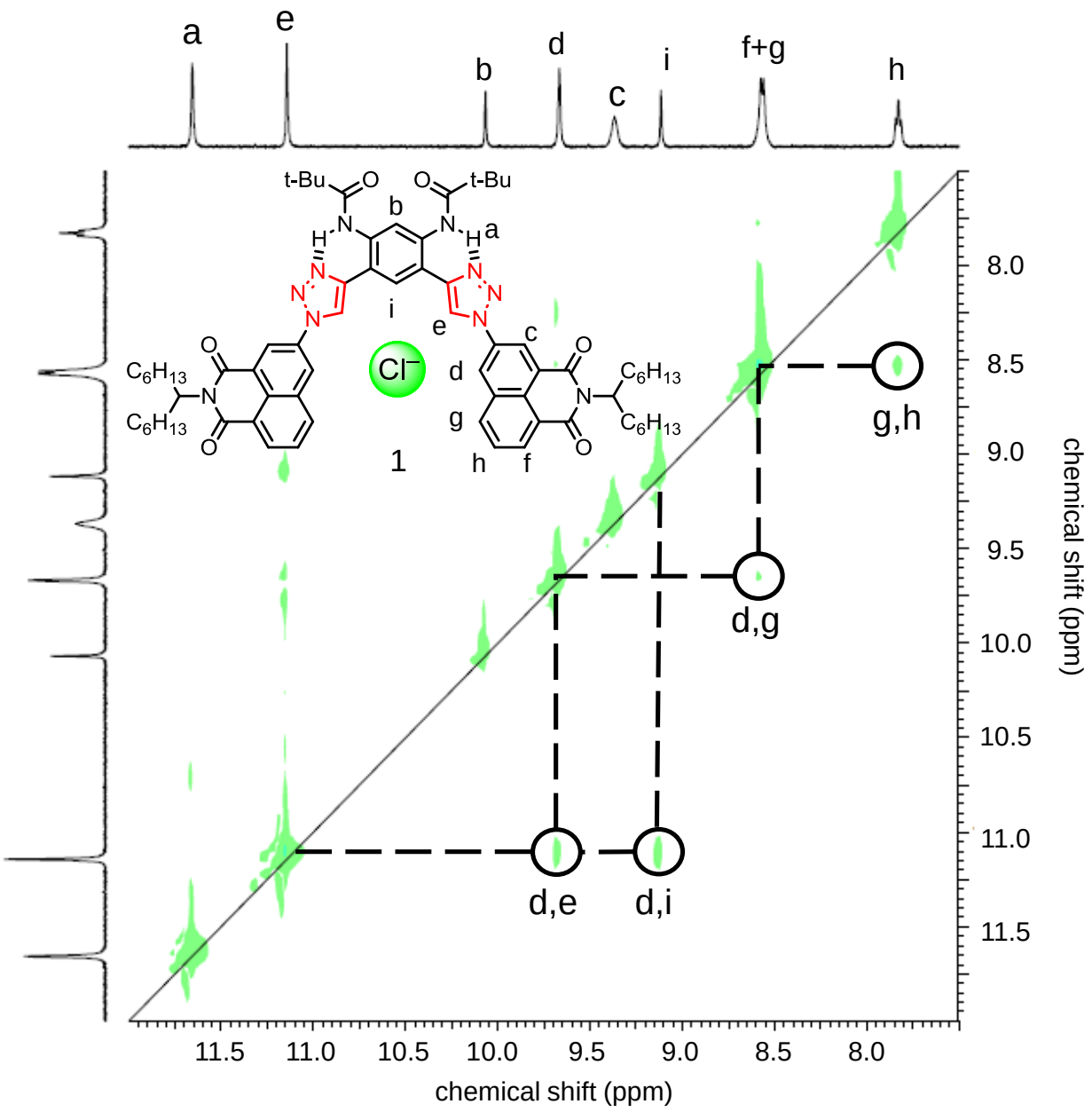

Figure S4. Aromatic region of 2D ROESY NMR on receptor **1** (~10 mM, CD_2Cl_2, 298 K) with added tetrabutylammonium chloride (10 equiv, TBACl).

S5. UV/Vis Titration Data and Sivvu Analysis – Receptor 1

Receptor **1** (or **2**) was dissolved in 3 mL CH_2Cl_2 in a screw-capped quartz cuvette (pathlength = 1 cm) and an initial UV spectrum (230 – 500 nm) was recorded. Aliquots of a TBA^+ halide solution (300-600 times more concentrated than the receptor solution) in CH_2Cl_2

was then added sequentially using a microsyringe through a rubber septum. After each addition, a UV spectrum was recorded.

The titrations (Figures S5, S9) were performed at low concentrations (2.5 – 10 μM) to allow the weaker species (**1**$_2$•X^-, **1**•TBA^+•X^-) to be omitted from the data fitting. Since the association constant (K_{ion}) for the TBA-halide salts in CH_2Cl_2 has been determined,[S6] these values were fixed in the data fitting software Sivvu[S7] to allow determination of K_1.

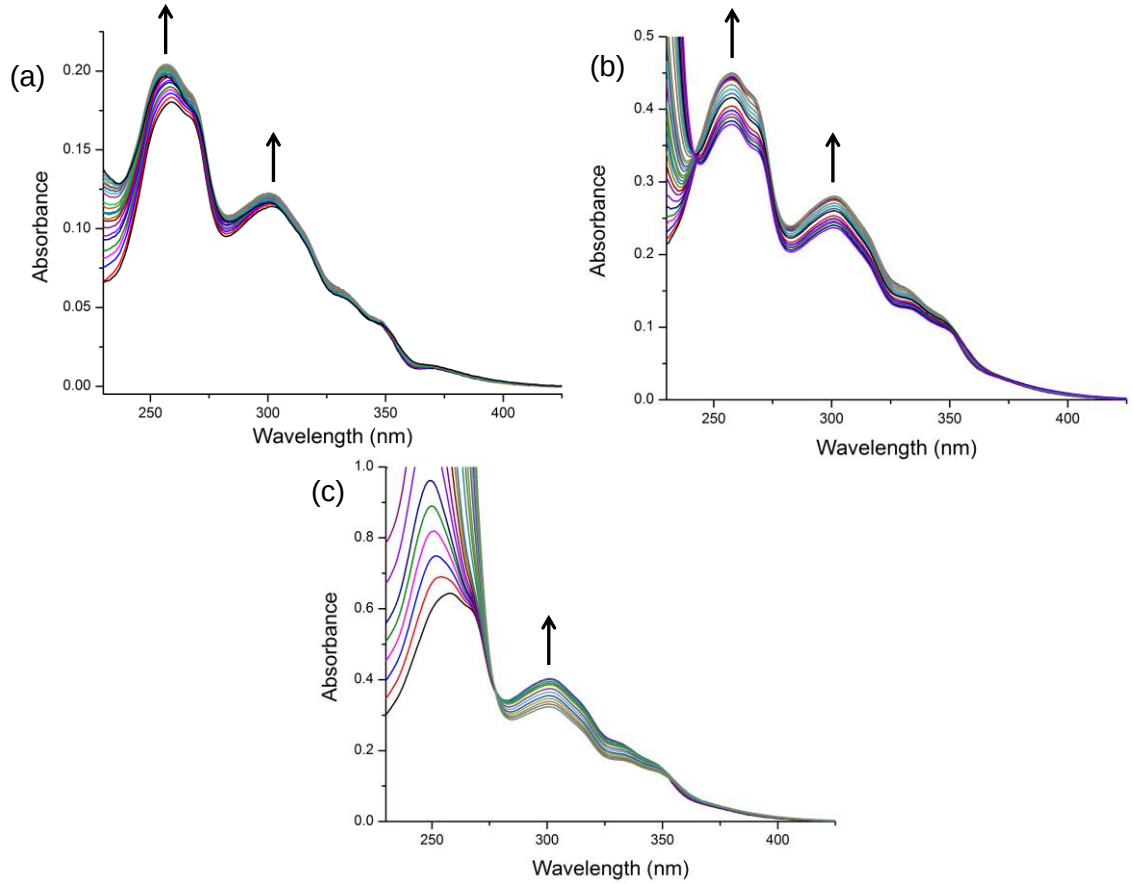

Figure S5. UV/Vis titrations of **1** (CH_2Cl_2) with (a) TBACl ([**1**] = 2.5 μM), (b) TBABr ([**1**] = 5.0 μM), and (c) TBAI ([**1**] = 10 μM). Arrows indicate observed changes in the absorption spectra upon sequential addition of anion.

Table S1. Data parameters used for SIVVU fitting of UV/Vis absorption data.

	λ range (nm)	Fixed absorbers	Fitted absorbers
1•Cl^-	270-450	**1**	**1**•Cl^-
1•Br^-	245-450	**1**	**1**•Br^-
1•I^-	275-400	**1**	**1**•I^- TBA^+I^-
2•Cl^-	250-400	**2**	**2**•Cl^-
2•Br^-	250-350	**2**	**2**•Br^-

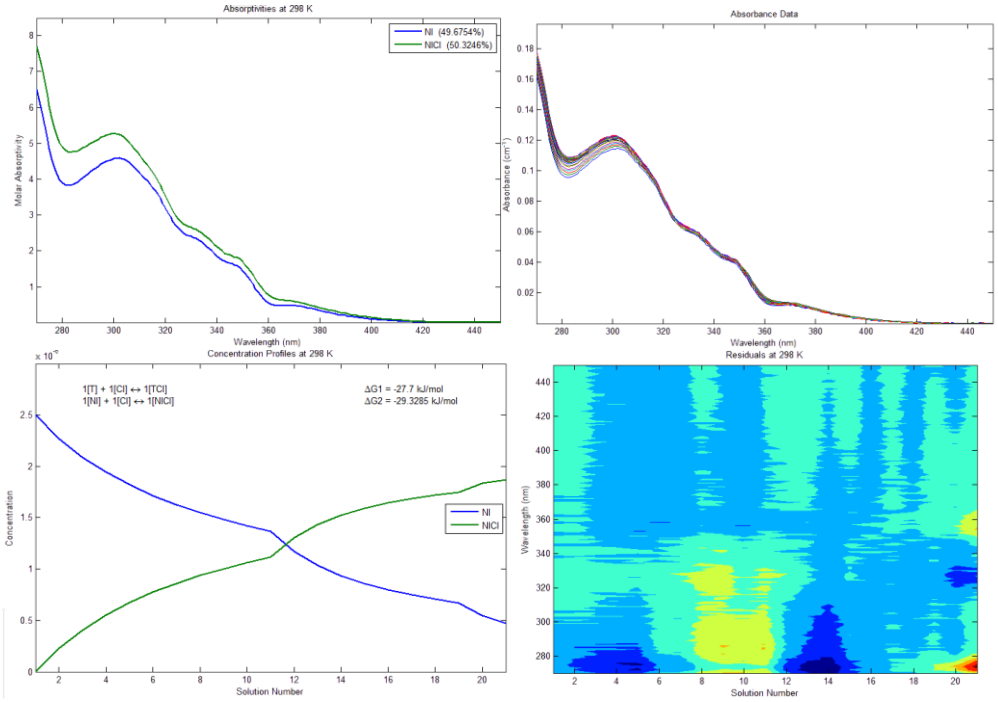

Figure S6. UV/Vis data fitting for **1**•Cl^- – K_1 determination

RMS Residual = 0.000307; Final R^2 = 99.9979%
Restricted Data Reconstruction (2 chemical factors): 99.1991%
Unrestricted Data Reconstruction (2 chemical factors): 99.3437%

The error of the UV data fitting by Sivvu was estimated by excluding random data points and then calculating the resulting binding energy. Three standard deviations were used for the error estimate listed in the main text (Table 1). This process of error estimation was used for all reported UV titrations.

Table S2. Binding energies (ΔG, kJ/mol) for **1**•Cl^- generated from the full data set and with randomly excluded data points.

Random Points Excluded	TBACl	**1**•Cl^-
none	–27.7	–29.3
4 6 12 13 15	–27.7	–29.4
3 10 11 13 15	–27.7	–29.3
3 6 9 12 20	–27.7	–29.3
4 8 18 19 21	–27.7	–29.6
4 9 10 15 17	–27.7	–29.2
3 5 6 17 18	–27.7	–29.4
Average	–27.7	–29.3
Std. Deviation		0.15

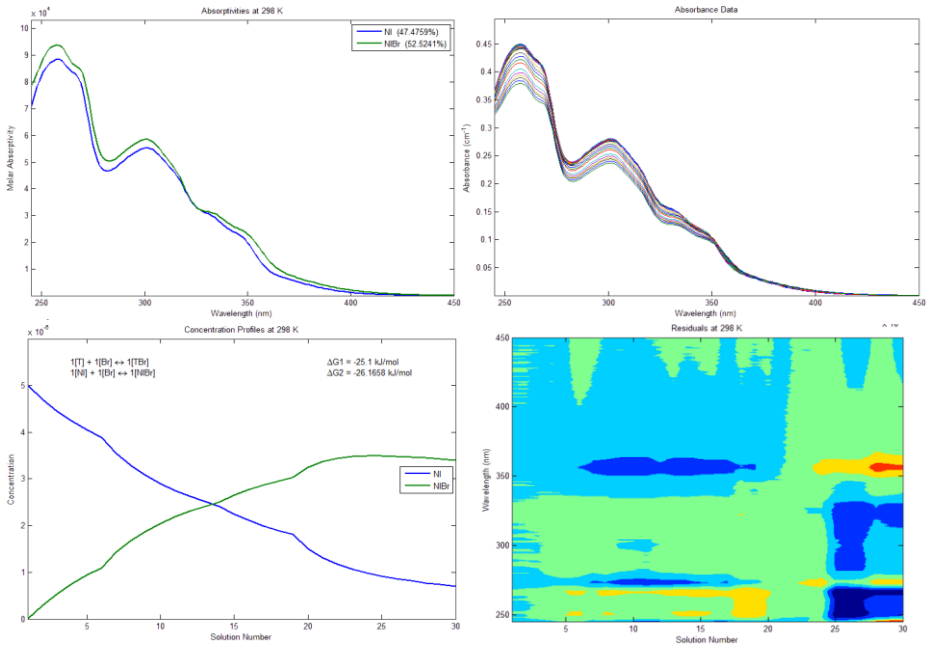

Figure S7. UV/Vis data fitting for **1**•Br^-

RMS Residual = 0.001263; Final R^2 = 99.996%
Restricted Data Reconstruction (2 chemical factors): 99.2295%
Unrestricted Data Reconstruction (2 chemical factors): 99.594%

Table S3. Binding energies (ΔG, kJ/mol) for **1**•Br^- generated from the full data set and with randomly excluded data points.

Random Points Excluded	TBABr	**1**•Br^-
none	–25.1	–26.2
15 16 18 22 26	–25.1	–26.0
10 12 15 23 29	–25.1	–26.3
15 16 25 26 30	–25.1	–26.0
2 5 13 20 28	–25.1	–26.2
9 13 16 28 29	–25.1	–26.3
6 7 18 22 24	–25.1	–26.2
3 12 13 18 30	–25.1	–26.2
Average	–25.1	–26.2
Std. Deviation		0.11

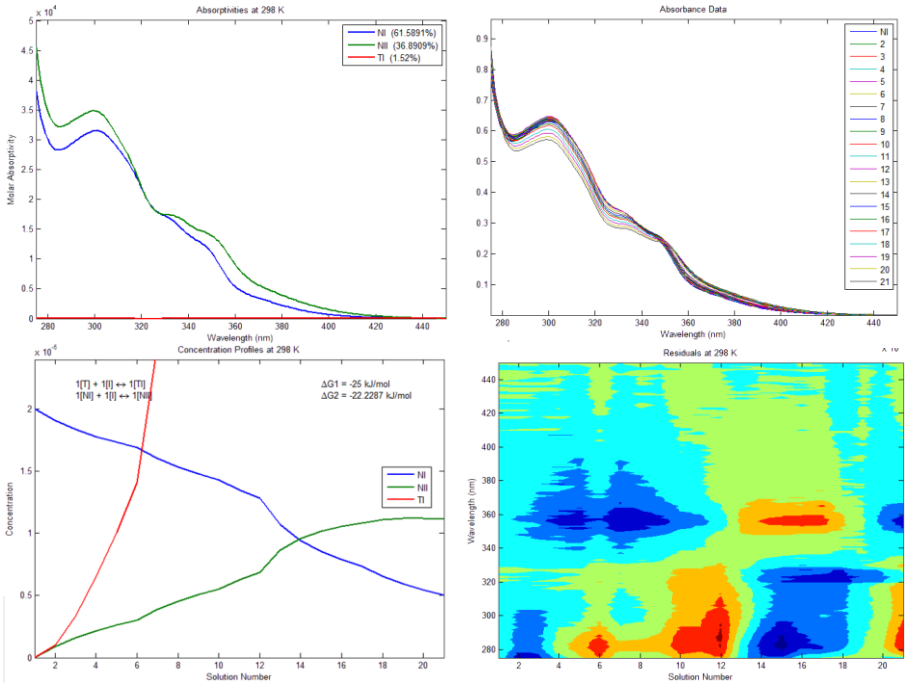

Figure S8. UV/Vis data fitting for **1**•I⁻

RMS Residual = 0.0003711; Final R^2 = 99.9996%
Restricted Data Reconstruction (3 chemical factors): 99.6938%
Unrestricted Data Reconstruction (3 chemical factors): 99.7028%

Error Analysis of Sivvu Fitting for 1•I⁻

Table S4. Binding energies (Δ*G*, kJ/mol) for **1**•I⁻ generated from the full data set and with randomly excluded data points.

Random Points Excluded	TBAI	**1**•I⁻
none	–25.0	–22.2
3 5 9 16 18	–25.0	–22.3
10 11 12 19 20	–25.0	–21.9
5 9 10 12 16	–25.0	–22.0
4 13 14 16 18	–25.0	–22.3
9 11 13 15 16	–25.0	–22.1
3 7 8 9 16	–25.0	–22.5
2 4 5 14 20	–25.0	–22.4
Average	–25.0	–22.2
Std. Deviation		0.21

S6. UV/Vis Titration Data and Sivvu Analysis – Receptor 2

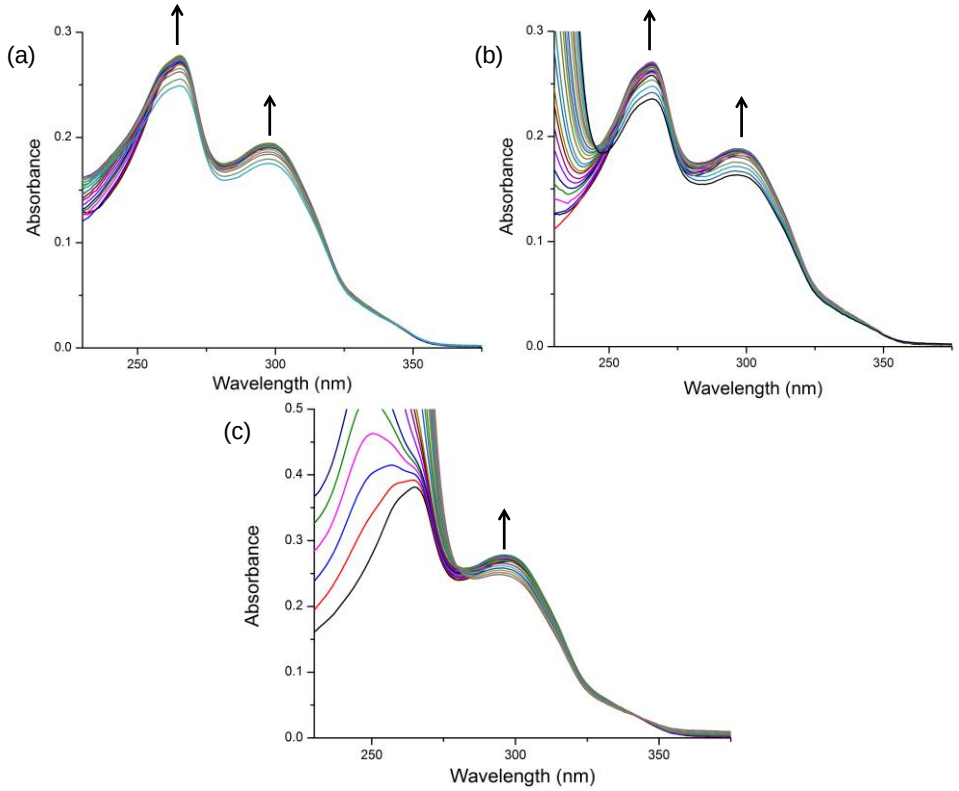

Figure S9. UV/Vis titrations of **2** (CH_2Cl_2) with (a) TBACl ([**2**] = 5 μM), (b) TBABr ([**2**] = 5 μM), and (c) TBAI ([**2**] = 10 μM). Arrows indicate observed changes in the absorption spectra upon sequential addition of anion.

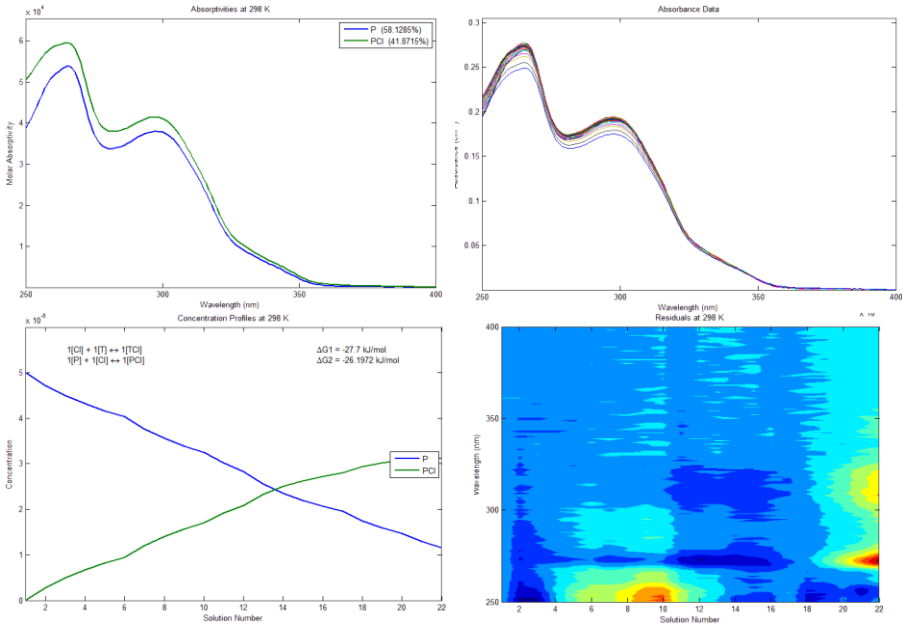

Figure S10. UV/Vis data fitting for **2**•Cl^-

RMS Residual = 0.001759; Final R^2 = 99.997%
Restricted Data Reconstruction (2 chemical factors): 99.596%
Unrestricted Data Reconstruction (2 chemical factors): 99.7105%

Error Analysis of Sivvu Fitting for 2•Cl^-

Table S5. Binding energies (ΔG, kJ/mol) for **2**•Cl^- generated from the full data set and with randomly excluded data points.

Random Points Excluded	TBACl	**2**•Cl^-
none	–27.7	–26.2
4 5 14 15 17	–27.7	–26.2
7 11 15 16 21	–27.7	–26.2
8 9 10 14 17	–27.7	–25.9
4 5 14 18 19	–27.7	–26.2
3 7 12 15 22	–27.7	–26.4
2 6 11 20 21	–27.7	–26.3
2 10 13 19 22	–27.7	–26.3
Average	–27.7	–26.2
Std. Deviation		0.17

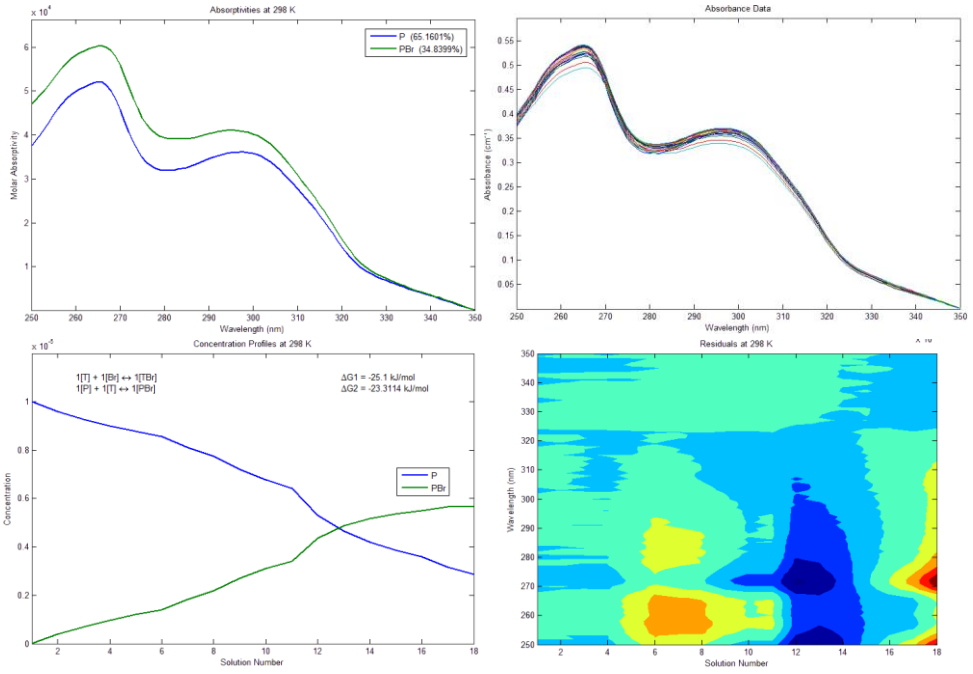

Figure S11. UV/Vis data fitting for **2**•Br^-

RMS Residual = 0.0005392; Final R^2 = 99.9983%

Restricted Data Reconstruction (2 chemical factors): 99.4831%
Unrestricted Data Reconstruction (2 chemical factors): 99.4882%

Error Analysis of Sivvu Fitting for 2•Br^-

Table S6. Binding energies (ΔG, kJ/mol) for **2**•Br^- generated from the full data set and with randomly excluded data points.

Random Points Excluded	TBABr	**2**•Br^-
none	–25.1	–23.3
5 6 9 10	–25.1	–22.9
7 9 12 18	–25.1	–23.7
2 3 6 10	–25.1	–23.1
2 5 8 13	–25.1	–23.1
4 7 14 16	–25.1	–23.1
3 7 8 13	–25.1	–23.0
3 4 7 9	–25.1	–23.0
Average	–25.1	–23.1
Std. Deviation		0.27

S7. ^{1}H NMR Titration Data and Analysis – Receptor 1

Receptor **1** (or **2**) was dissolved in 400 μL CD_2Cl_2 in an NMR tube sealed with a rubber septum. An initial ^{1}H NMR spectrum was recorded and additional spectra were obtained after aliquots of a TBA^+ halide solution (in CD_2Cl_2) was injected sequentially using a microsyringe. The ^{1}H NMR peak data was then fit according to the four equilibria (K_1, K_2, K_{ion}, K_{ipc}) using HypNMR.[S8]

Data Fitting – HypNMR

As discussed in the main text, HypNMR[S8] was used to fit the ^{1}H NMR titration data to four equilibria: K_1, K_2, K_{ion}, and K_{ipc}. To simplify the fitting, the K_1 values were obtained separately through a UV/Vis titration (Figures S5–S11). Performing the titrations at UV/Vis concentrations (<10 μM) allowed the weaker K_2 and K_{ipc} equilibria to be omitted (Figures S20-S24). The presence of K_2 and K_{ipc} at NMR concentrations (>500 μM) are rationalized by ESI-MS experiments (Figure S25-26) and literature precedence.[S5] Excluding either of these equilibria in a global fitting of the ^{1}H NMR data resulted in illogical K values that did not support the experimental data.

While UV/Vis titrations allowed quantitative and *accurate* determination of the 1:1 binding constants, experimental conditions (in CH_2Cl_2) do not allow the K_2 and K_{ipc} values to be separated from another. Since these binding constants are weak compared to competitive ion binding, the accuracy of their determination is limited and little information can be gained from

their experimental values. Accordingly, the associated errors on these values are high. The reported fitting was obtained through a combination of systematic variation and chemical intuition. For titrations on receptor **1**, the fitting did not converge when both K_2 and K_{ipc} were allowed to be refined by HypNMR (K_{ion}[S9] and K_1 were fixed). To provide an estimation of these binding constants, K_{ipc} was fixed at a possible value thus allowing the software to refine K_2. This strategy was utilized in prior work on triazolophanes.[S5] Acceptable values for K_{ipc} were rationalized based on the calculated chemical shifts for each complex (**1**•X^-, $\mathbf{1}_2$•X^-, **1**•T^+•X^-, and T^+•X^-). Although these values are algebraic fits according to the calculated concentration of each species in solution, those that presented unrealistic chemical shift positions were discarded as erroneous results. The corresponding range of accepted values (Figures S15 and S19) that were used in the global fitting of the ^{1}H NMR data is represented as colored boxes.

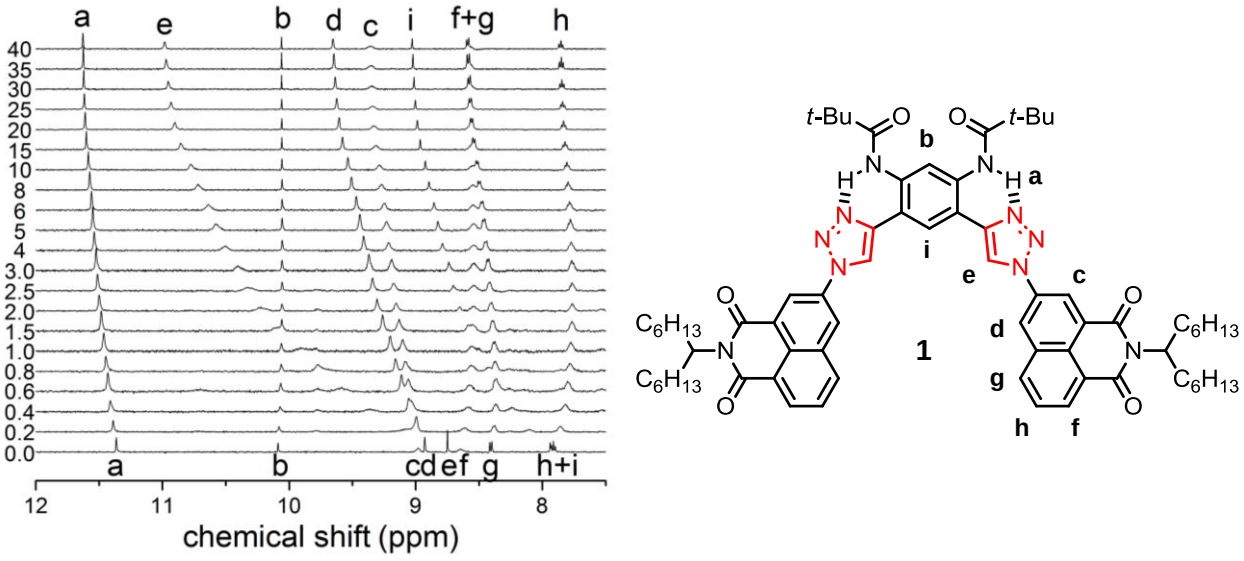

Figure S12. ^{1}H NMR titration of **1** (500 μM, CD_2Cl_2) with increasing equivalents of TBACl added.

HypNMR2008 Output:

Sigma = 5.262456

	value	standard deviation
log beta(TCl)	4.86	fixed
log beta(NICl)	5.136	fixed
log beta(NI_2Cl)	9.0507	0.0569
log beta(NITCl)	8.0	fixed

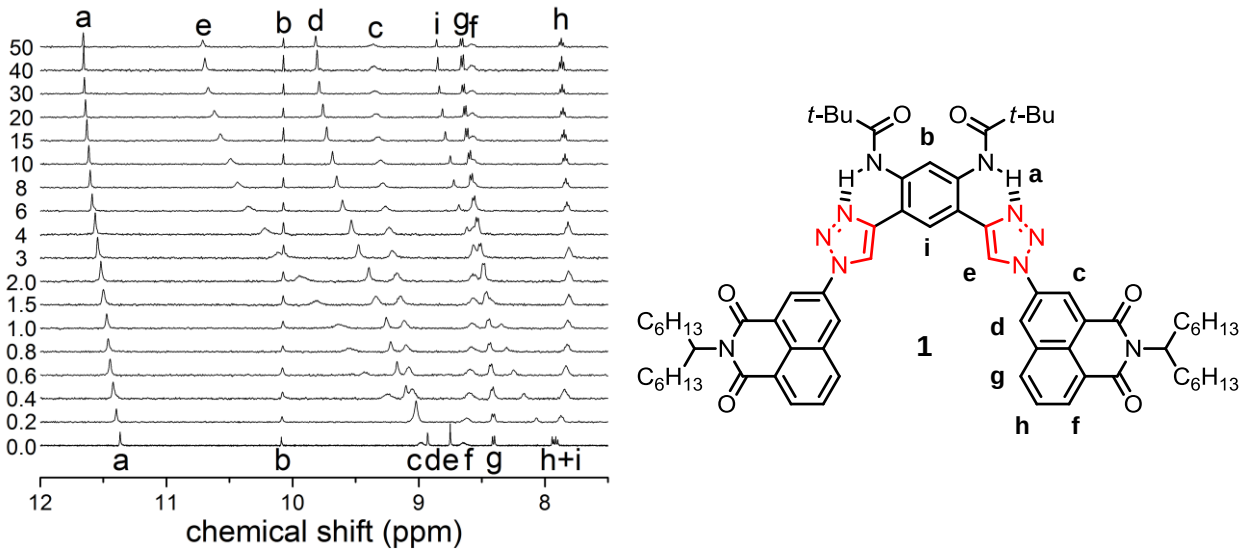

Figure S13. ^{1}H NMR titration of **1** (500 μM, CD_2Cl_2) with increasing equivalents of TBABr added.

HypNMR2008 Output:

Sigma = 5.142436

	value	standard deviation
log beta(TBr)	4.4	fixed
log beta(NIBr)	4.59	fixed
log beta(NI_2Br)	8.0663	0.0863
log beta(NITBr)	7.3	fixed

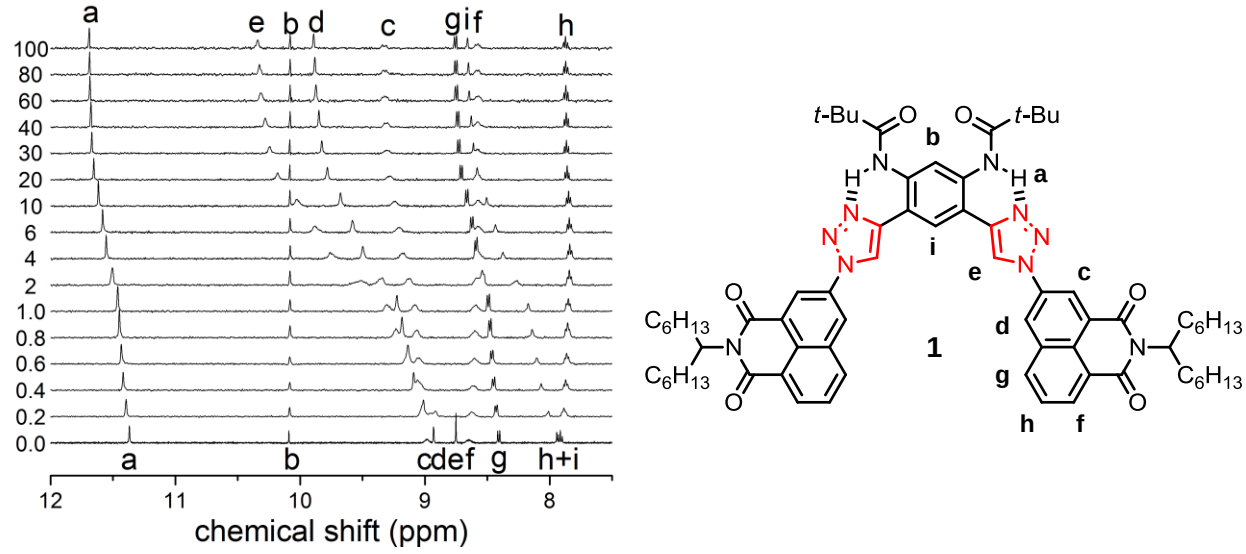

Figure S14. ^{1}H NMR titration of **1** (500 μM, CD_2Cl_2) with increasing equivalents of TBAI added

HypNMR2008 Output:

Sigma = 3.255279

	value	standard deviation
log beta(TI)	4.38	fixed
log beta(NII)	3.91	fixed
log beta(NI_2I)	7.414	0.0752
log beta(NITI)	6.88	fixed

Table S7. Observed chemical shift changes for **1**•X^- complexes

	$\Delta\delta$ (**1**, H_e)	$\Delta\delta$ (**1**, H_i)	$\Delta\delta$ (**1**, H_d)	$\Delta\delta$ (**1**, H_g)
Cl^-	2.24	1.09	0.73	0.18
Br^-	1.96	0.92	0.89	0.25
I^-	1.59	0.72	0.96	0.35

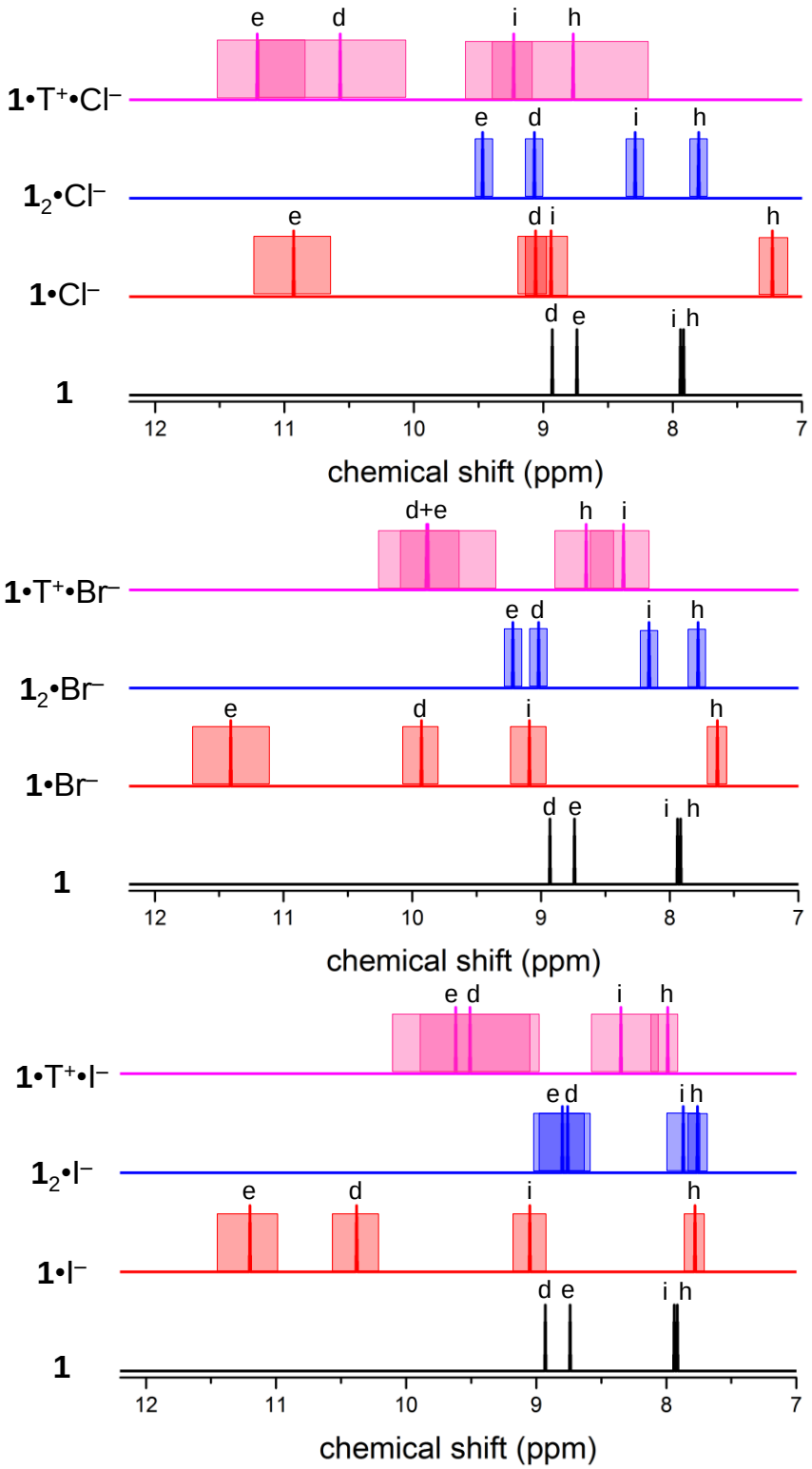

Figure S15. Calculated chemical shift of each nucleus within **1** and its various complexes obtained from HypNMR data fitting. The colored boxes indicate the acceptable range of chemical shift values obtained from the systematic global fitting of the ^{1}H NMR data.

S8. ^{1}H NMR Titration Data and Analysis – Receptor 2

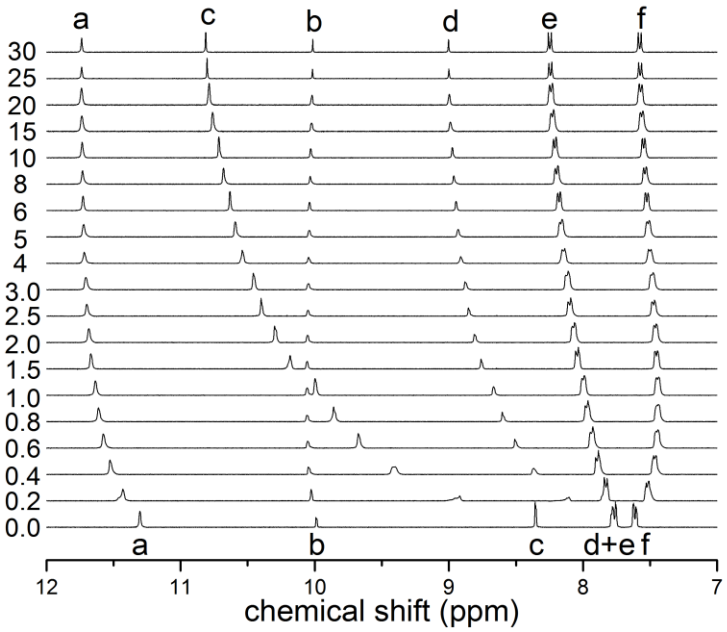

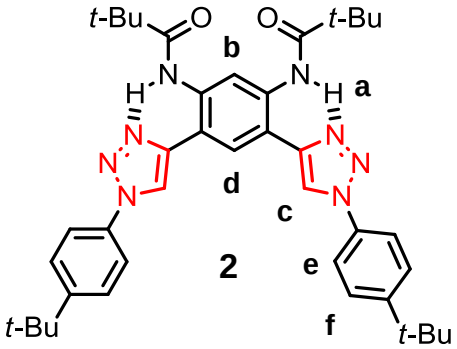

Figure S16. ^{1}H NMR titration of **2** (5 mM, CD_2Cl_2) with increasing equivalents of TBACl added.

HypNMR2008 Output:

Sigma = 10.8189

	value	standard deviation
log beta(TCl)	4.86	fixed
log beta(PCl)	4.59	fixed
log beta(P_2Cl)	7.182	0.0816
log beta(PTCl)	6.9	fixed

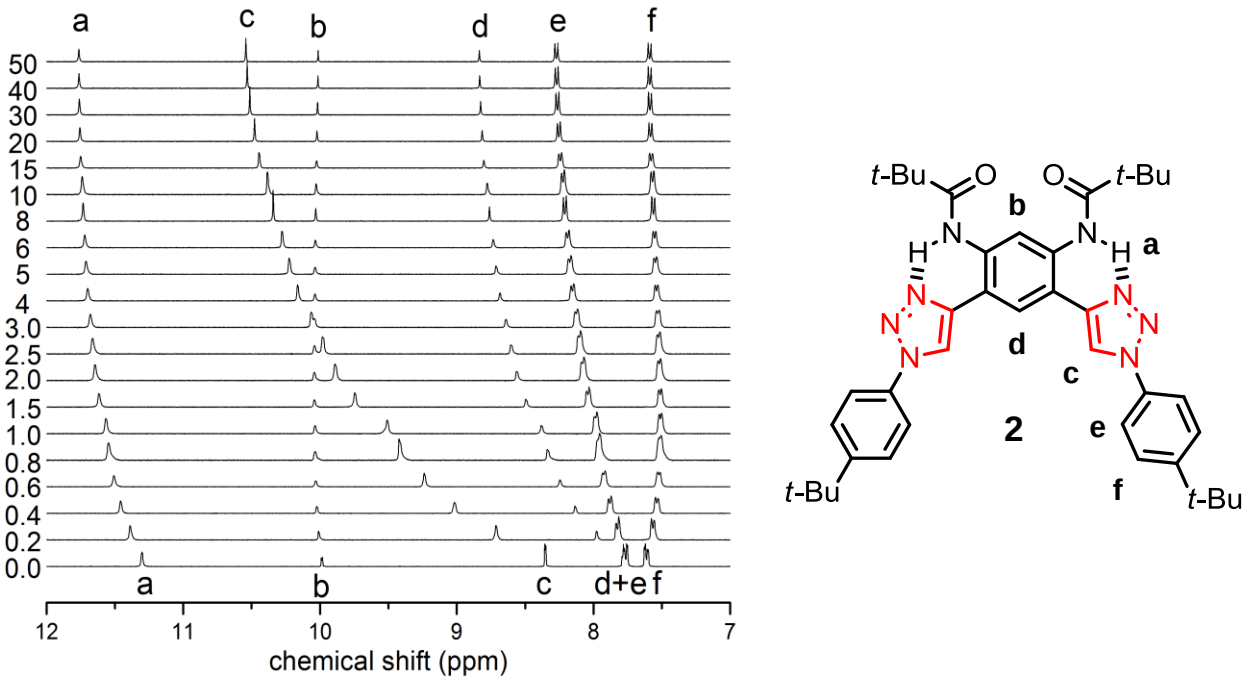

Figure S17. ^{1}H NMR titration of **2** (5 mM, CD_2Cl_2) with increasing equivalents of TBABr added.

HypNMR2008 Output:

Sigma = 5.044873

	value	standard deviation
log beta(TBr)	4.4	fixed
log beta(PBr)	4.04	fixed
log beta(P2Br)	7.044	0.074
log beta(PTBr)	6.992	0.039

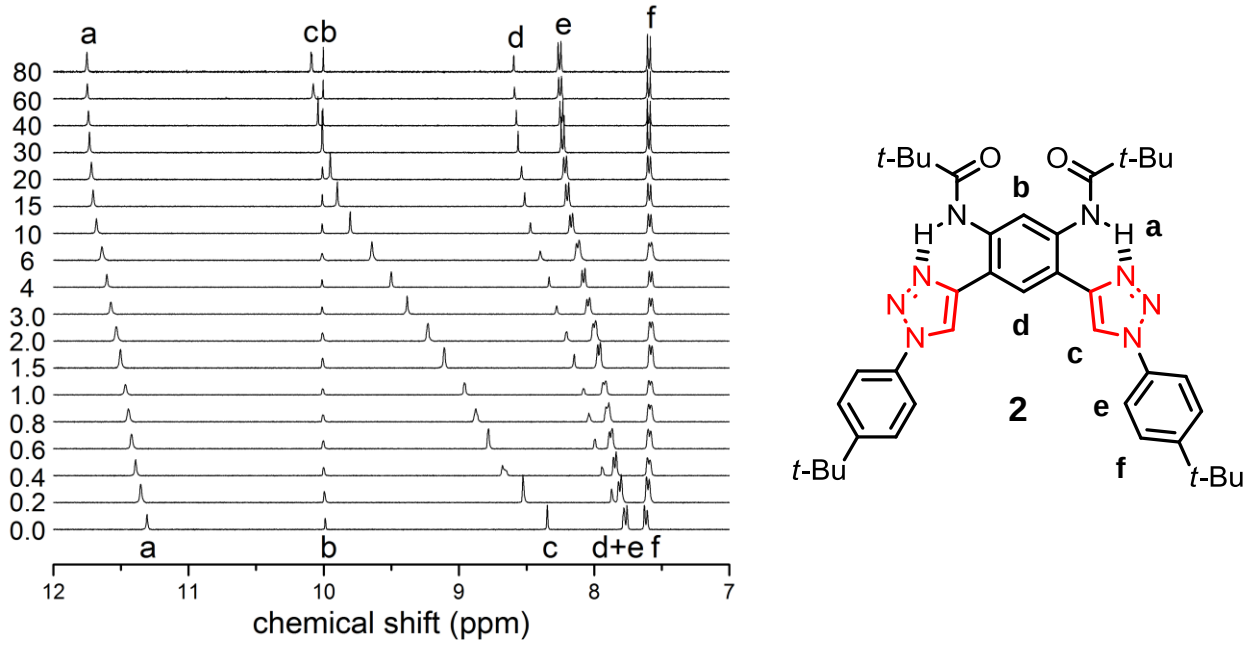

Figure S18. ^{1}H NMR titration of **2** (5 mM, CD_2Cl_2) with increasing equivalents of TBAI added.

Since a reliable value for the 1:1 binding constant for **2**•I^- (using UV/Vis titration) could not be determined, fitting of the HypNMR data to determine K_2 and K_{ipc} was unsuccessful. The UV/Vis titration was complicated by (1) absorption of TBAI and (2) competitive ion-pairing even at lower concentrations. A high of excess of TBAI (>150 equivalents) was required to saturate the receptor (20 μM). Simulation of this qualitative observation using Hyss2009 leads to a maximum approximation for the iodide binding constant of 1,000 M^{-1}.

Table S8. Observed chemical shift changes for **2**•X^- complexes

	$\Delta\delta$ (**2**, H_c)	$\Delta\delta$ (**2**, H_d)	$\Delta\delta$ (**2**, H_e)
Cl^-	2.46	1.21	0.48
Br^-	2.19	1.05	0.51
I^-	1.74	0.82	0.49

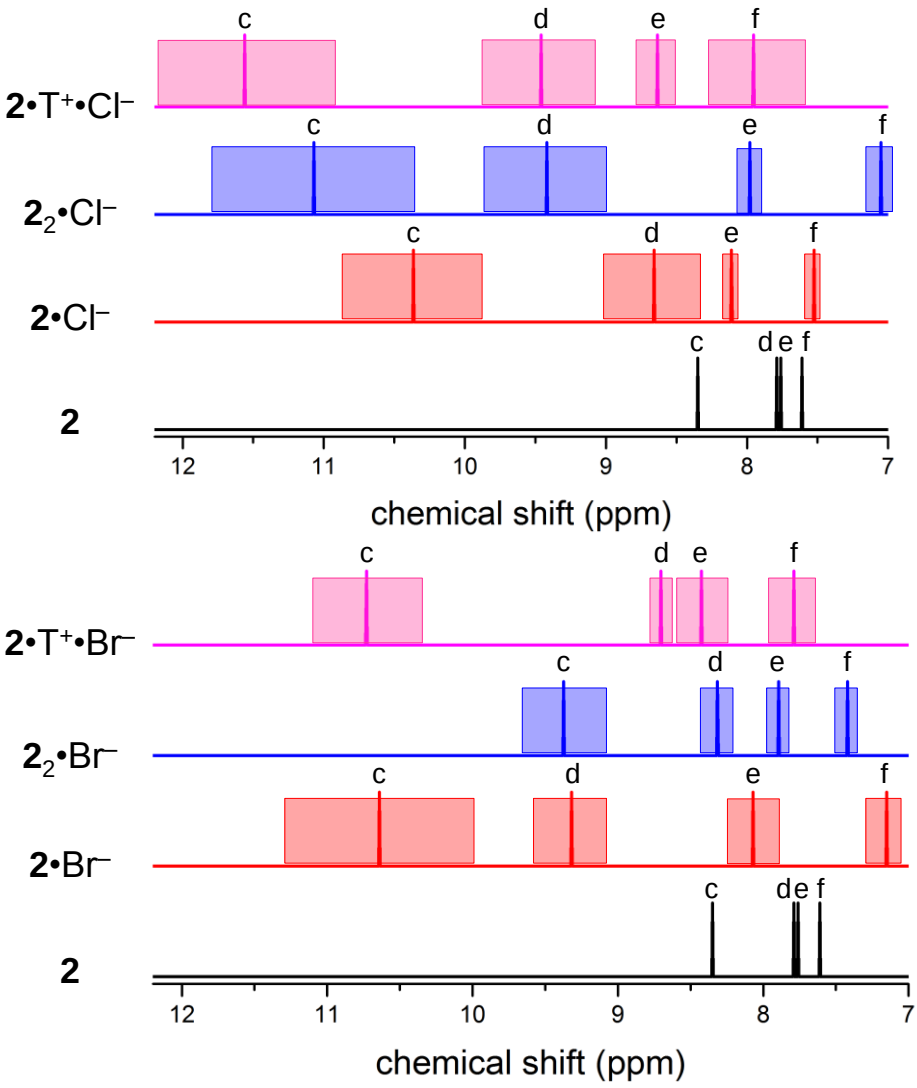

Figure S19. Calculated chemical shift of each nucleus within **2** and its various complexes obtained from HypNMR data fitting. The colored boxes indicate the acceptable range of chemical shift values obtained from the systematic global fitting of the ^{1}H NMR data.

Table S9. Calculated binding constants (M^{-1}) and free energies (kJ/mol) for receptors **1**

	K_1 (**1**, UV)	K_2 (**1**, NMR)	K_{ipc} (**1**, NMR)	K_{ion} (**1**)
	ΔG_1 (**1**•X^-)	ΔG_2 (**1**$_2$•X^-)	ΔG_{ipc} (**1**•T^+•X^-)	ΔG_{ion} (T^+•Cl^-)
Cl^-	14 ±0.2 × 10^4	2 ±1 × 10^4	3 ±2 × 10^3	7.2 ±0.5 × 10^4
	–29.3 ± 0.4	–25 ±2	–20 ±3	–27.7 ±0.2
Br^-	3.9 ±0.5 × 10^4	5 ±2 × 10^3	1.2 ±0.7 × 10^3	2.5 ±0.2 × 10^4
	–26.2 ±0.3	–21 ±1	–18 ±2	–25.1 ±0.2
I^-	7.8 ±0.1 × 10^3	3 ±1 × 10^3	1.1 ±0.6 × 10^3	2.4 ±0.2 × 10^4
	–22.2 ± 0.6	–20 ±1	–17 ±2	–25.0 ±0.2

Table S10. Calculated binding constants (M^{-1}) and free energies (kJ/mol) for receptors **1**

	K_1 (**2**, UV)	K_2 (**2**, NMR)	K_{ipc} (**2**, NMR)	K_{ion} (**2**)
	ΔG_1 (**2**•X^-)	ΔG_2 (**2**$_2$•X^-)	ΔG_{ipc} (**2**•T^+•X^-)	ΔG_{ion} (T^+•X^-)
Cl^-	$4.2 \pm 0.2 \times 10^4$	$6 \pm 4 \times 10^2$	$3 \pm 2 \times 10^2$	$7.2 \pm 0.5 \times 10^4$
	–26.3 ± 0.1	–16 ±3	–14 ±3	–27.7 ±0.2
Br^-	$1.1 \pm 0.2 \times 10^4$	$1.0 \pm 0.6 \times 10^3$	$1.9 \pm 1.5 \times 10^3$	$2.5 \pm 0.2 \times 10^4$
	–23.1 ±0.2	–17 ±1	–19 ±4	–25.1 ±0.2

Simulated Speciation Curves

Speciation curves were generated using Hyss2009 according to the experimentally determined binding constants from UV/Vis and 1H NMR titrations. It is evident from these plots that the weaker ion complexes (K_2, K_{ipc}) can be omitted from the analysis at lower concentrations (<10 uM).

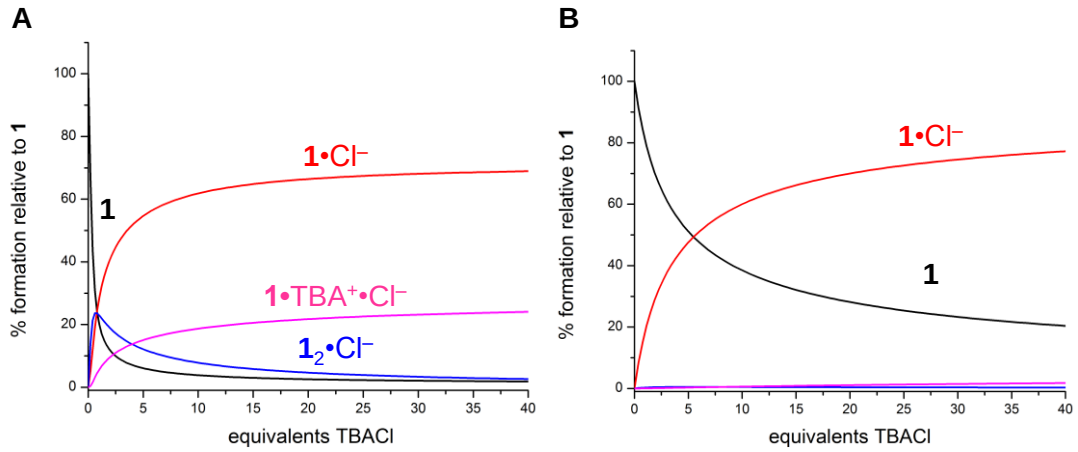

Figure S20. Simulated speciation curves for **1**•Cl^- @ 500 μM (**A**) and 2.5 μM (**B**)

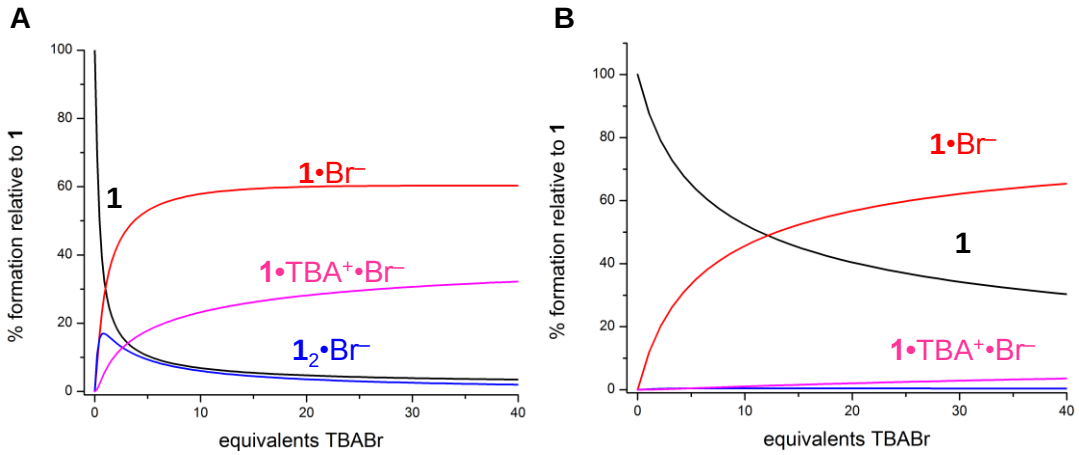

Figure S21. Simulated speciation curves for **1**•Br^- @ 500 μM (**A**) and 5 μM (**B**)

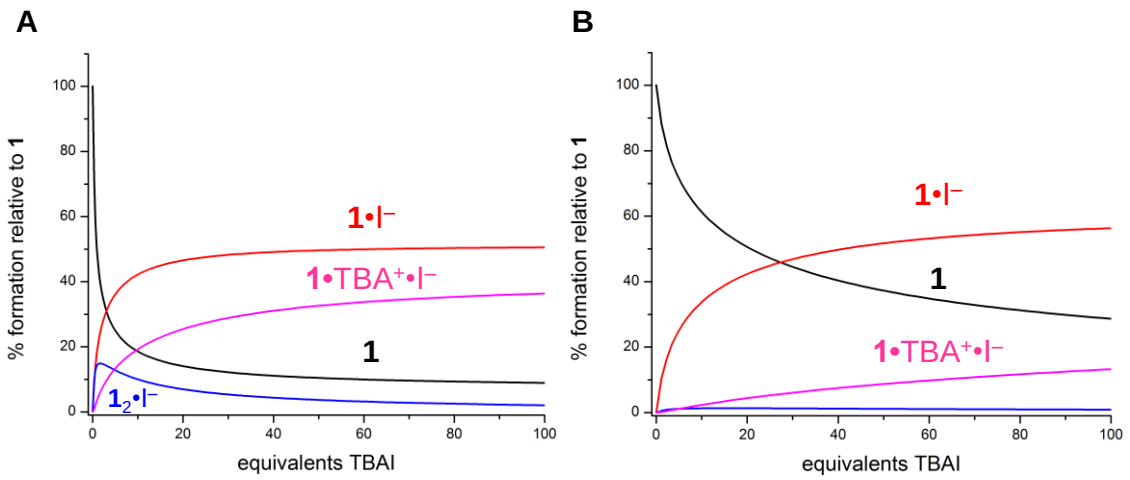

Figure S22. Simulated speciation curves for **1**•I⁻ @ 500 μM (**A**) and 10 μM (**B**)

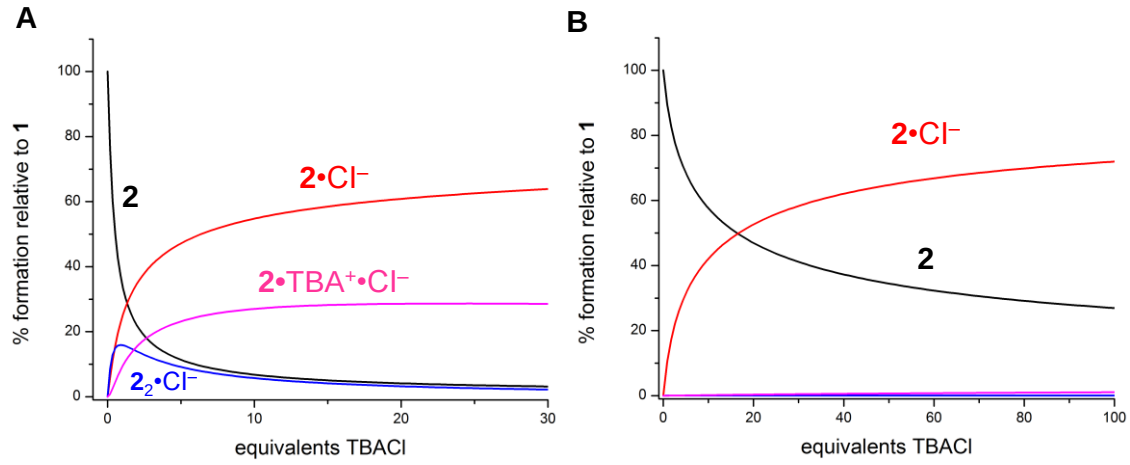

Figure S23. Simulated speciation curves for **2**•Cl⁻ @ 5 mM (**A**) and 5 μM (**B**)

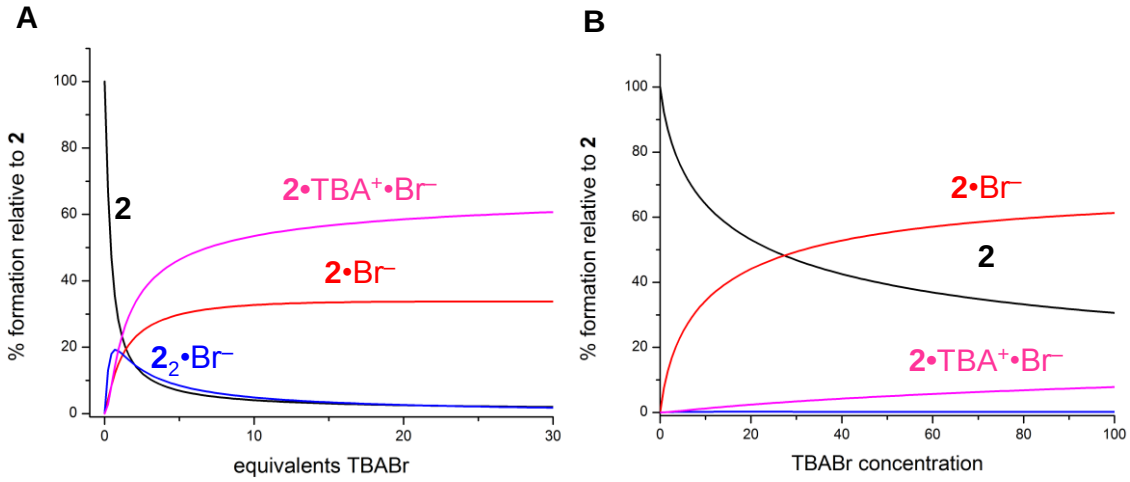

Figure S24. Simulated speciation curves for **2**•Br⁻ @ 5 mM (**A**) and 10 μM (**B**)

S10. Electrospray Ionization Mass Spectroscopy – Confirmation of 1:1 and 2:1 Host:Guest Complexes

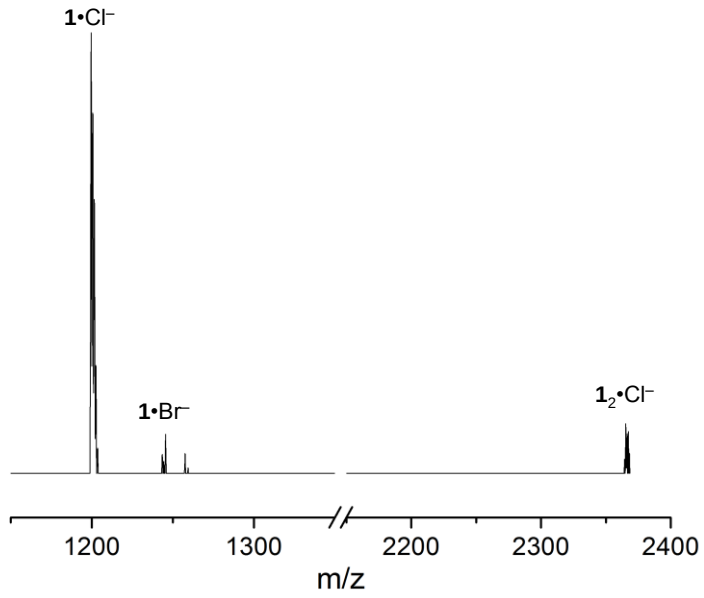

Figure S25. ESI-MS spectrum titration of **1** (~10 μM, CH_2Cl_2) with 0.5 equivalent of TBACl added. Note: the observed **1**•Br^- signal is attributed to **1** scavenging bromide from within the ESI-MS instrument.

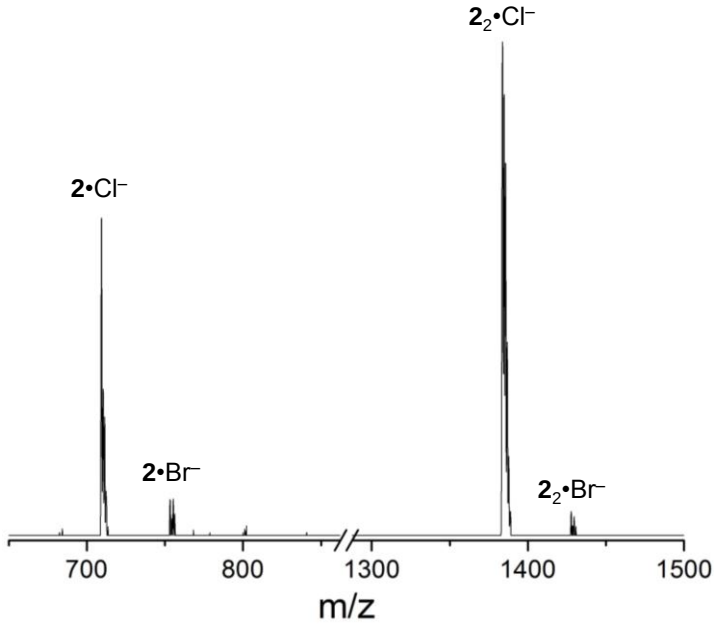

Figure S26. ESI-MS spectrum titration of **2** (~10 μM, CH_2Cl_2) with 0.5 equivalent of TBACl added. Note: the observed **2**•Br^- and $\mathbf{2}_2$•Br^- signal is attributed to **2** scavenging bromide, again, from within the ESI-MS instrument

S11. Computational Analysis of 1•Cl⁻, 1•Br⁻, and 2•Cl⁻ complexes

Table S11. Calculated (B3LYP/6-31+G(d,p)) hydrogen bond distances for receptor-halide complexes.

	CH•••X (triazole)[a]	CH•••X (phen)[a]	CH•••X (NI –C^4)[a]	CH•••X (NI –C^5)[a]	CH•••X (**2**, phen)[a]	Σ (vdW)
1•Cl⁻	2.48	3.04	2.56	3.49		2.87
2•Cl⁻	2.40	2.88			2.67	2.87
1•Br⁻	2.63	3.23	2.56	3.33		3.02

[a]Values reported in angstroms

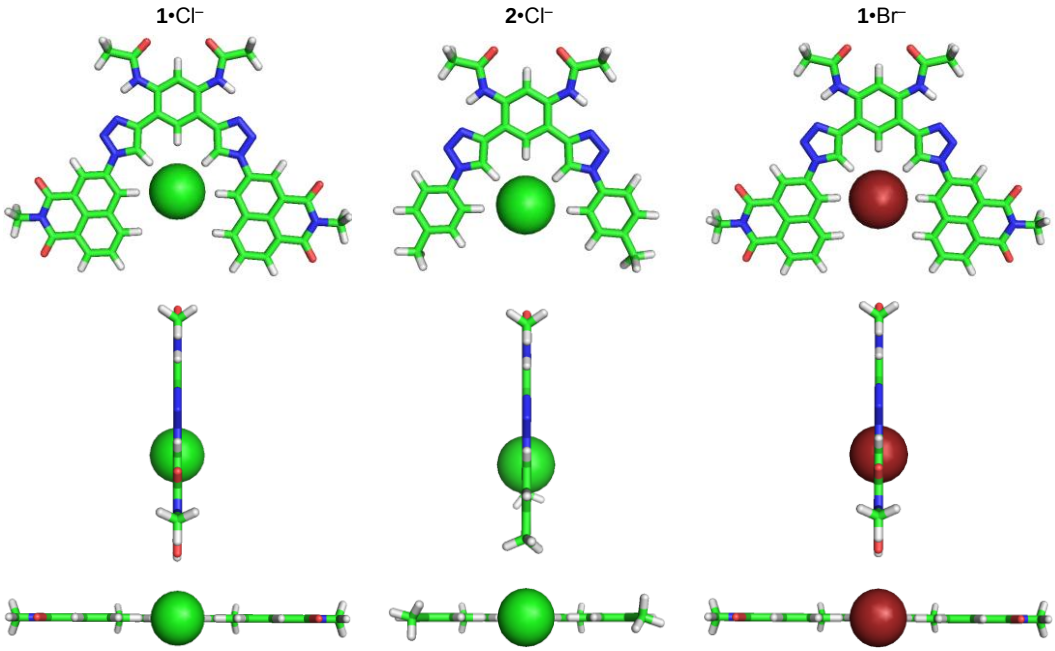

Figure S27. Geometry optimized (B3LYP/6-31+G(d,p)) structures for **1**•Cl⁻, **2**•Cl⁻, and **1**•Br⁻

Table S12. Calculated (B3LYP/6-31+G(d,p)) hydrogen bond distances and binding energies (B3LYP/6-311+G(3df,2p)) for naphthalimide (**NI**) and triazole (**T**) chloride complexes.

	Δ*E* (kJ/mol)	CH•••X⁻ (**NI**, C^4–H)[a]	CH•••X⁻ (**NI**, C^5–H)[a]	CH•••X⁻ (**T**, C^4–H)[a]	∠CH•••X⁻ (°)
NI•Cl⁻ (bifurcated)	–80	2.51	2.51		153.4, 153.4
NI•Cl⁻ (linear)	–72	2.22	3.34		180, 131.5
T•Cl⁻	–64			2.33	180

[a]Values reported in angstroms

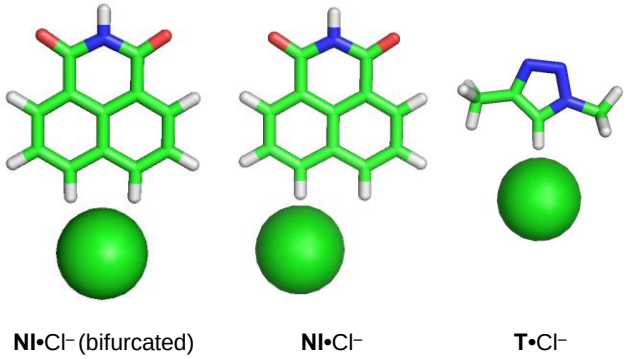

Figure S28. Geometry optimized (B3LYP/6-31+G(d,p)) structures for **NI**•Cl^- (bifurcated and linear) and **T**•Cl^-.

S12. Stabilization Gained From Individual CH Donors of 1,8-Naphthalimide

While the "urea-like" donor array of naphthalimide (**NI**) is evident from the preceding gas phase calculations, the differing roles of the C^4–H and C^5–H hydrogen bonds in receptor **1** prompted a brief investigation into the effect of the proximal C^5–H donor. To explore this with DFT calculations, the naphthalimide ring (**NI**) was deconstructed into model compound **NI–C^4** (Figure S29). This removes the proximal C^5 donor while maintaining polarization of the C^4 donor from the electron-withdrawing imide. Comparing the binding energy of constrained **NI–C^4** (ΔE = –58 kJ/mol) to **NI** (ΔE = –72 kJ/mol) shows that the C^5 donor is responsible for ~20% of the electronic stabilization provided by the naphthalimide unit.

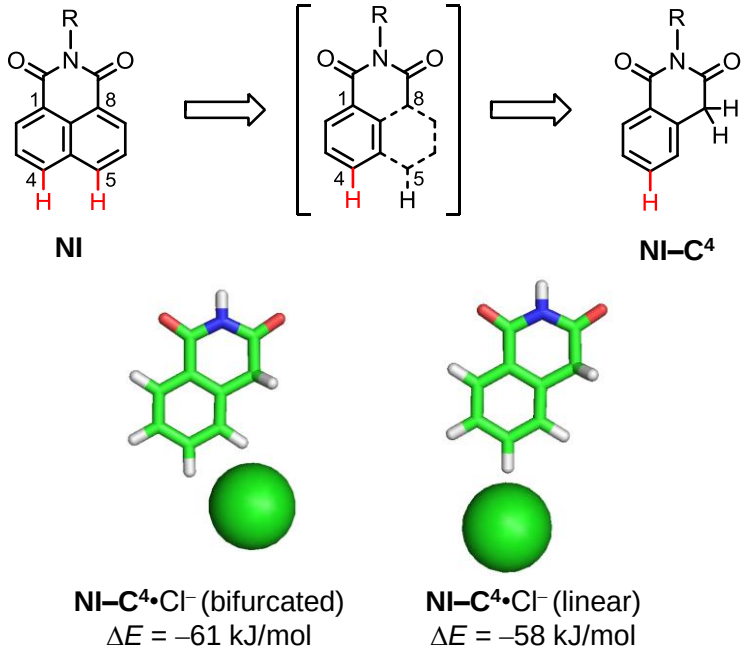

Figure S29. Geometry optimized (B3LYP/6-31+G(d,p)) structures and binding energies (B3LYP/6-311+G(3df,2p)) for **NI-C^4**•Cl^- provide insight into the importance of the C^5–H donor in the "urea-like" binding array of the naphthalimide ring.

S13. Computational Details

Density functional theory (DFT) calculations in the gas phase have been carried out using the *Gaussian 09*[S10] suite of programs. All the geometries have been optimized using the standard B3LYP[S11] density functional with the 6-31+G(d,p) basis set. Vibrational frequencies have been evaluated using the 6-31+G(d,p) basis set. Unless stated, all the structures are confirmed to be minimum energy structures with no imaginary frequencies. Single point energy calculations were then carried out using the significantly larger 6-311++G(3df,2p) basis set to obtain the anion binding energies. The binding energies were corrected for basis set superposition errors (BSSE) using the standard counterpoise method.[S12] Since both **NI**•Cl^- and **T**•Cl^- prefer the bifurcated mode of CH hydrogen bonding, a constrained optimization (B3LYP/6-31+G(d,p)) was performed on both **NI**•Cl^- and **T**•Cl^- to obtain the linear modes of CH hydrogen bonding.

References

(S1) Lee, J.-J.; Noll, B. C.; Smith, B. D. *Org. Lett.* **2008**, *10*, 1735-1738.

(S2) Holman, M. W.; Liu, R.; Adams, D. M. J. Am. Chem. Soc. **2003**, *125*, 12649-12654.

(S3) Lee, S.; Hua, Y.; Park, H. Flood, A. H. *Org. Lett.* **2010**, *12*, 2100-2101

(S4) Hua, Y.; Ramabhadran, R. O.; Karty, J. A.; Raghavachari, K.; Flood, A. H. *Chem. Commun.* **2011**, *47*, 5979-5981.

(S5) Hua, Y.; Ramabhadran, R. O.; Uduehi, E. O.; Karty, J. A.; Raghavachari, K.; Flood, A. H. *Chem. Eur. J.* **2011**, *17*, 312-321.

(S6) Svorstøl, I.; Høiland, H.; Songstad, J. *Acta. Chem. Scand. B*. **1984**, *10*, 885-893.

(S7) Vander Griend, D. A.; Bediako, D. K.; DeVries, M. J.; Dejoing, N. A.; Heeringa, L. P. *Inorg. Chem.* **2008**, *47*, 656-662.

(S8) Frassineti, C.; Ghelli, S.; Gans, P.; Sabatina, A.; Moruzzi, M. S.;Vacca, A. *Anal. Biochem*. **1995**, *231*, 374-382.

(S9) Svorstøl, I.; Høiland, H.; Songstad, J. *Acta. Chem. Scand. B.* **1984**, *10*, 885-893

(S10) M. J. Frisch, G. W. T., H. B. Schlegel, G. E. Scuseria, M. A. Robb, J. R. Cheeseman, G. Scalmani, V. Barone, B. Mennucci, G. A. Petersson, H. Nakatsuji, M. Caricato, X. Li, H. P. Hratchian, A. F. Izmaylov, J. Bloino, G. Zheng, J. L. Sonnenberg, M. Hada, M. Ehara, K. Toyota, R. Fukuda, J. Hasegawa, M. Ishida, T. Nakajima, Y. Honda, O. Kitao, H. Nakai, T. Vreven, J. A. Montgomery, Jr., J. E. Peralta, F. Ogliaro, M. Bearpark, J. J. Heyd, E. Brothers, K. N. Kudin, V. N. Staroverov, R. Kobayashi, J. Normand, ; K. Raghavachari, A. R., J. C. Burant, S. S. Iyengar, J. Tomasi, M. Cossi, N. Rega, J. M. Millam, M. Klene, J. E. Knox, J. B. Cross, V. Bakken, C. Adamo, J. Jaramillo, R. Gomperts, R. E. Stratmann, O. Yazyev, A. J. Austin, R. Cammi, C. Pomelli, J. W. Ochterski, R. L. Martin, K. Morokuma, V. G. Zakrzewski, G. A. Voth, P. Salvador, J. J. Dannenberg, S. Dapprich, A. D. Daniels, O. Farkas, J. B. Foresman, J. V. Ortiz, J. Cioslowski, and D. J. Fox; Gaussian-09, *Gaussian, Inc*.: Wallingford CT, 2009.

(S11) (a) Becke, A. D. *J. Chem. Phys.* **1993**, *98*, 5648-5652. (b) Lee, C. T.; Yang, W. T.; Parr, R. G. *Phys. Rev. B* **1988**, *37*, 785-789.

(S12) Mayor, I.; Surjan, P. R. *Chem. Phys. Lett*. **1992**, *191*, 497.